STATIC EARTHQUAKE TRIGGERING OF CENTRAL HIMALAYA IN PAKISTAN REGION BY COULOMB FAILURE

FAIZA GHOUS

Mphil. Geophysics

(2020-2022)

Department of Earth Sciences

Quaid-i-Azam University

Islamabad, Pakistan.

CERTIFICATE OF APPROVAL

This dissertation by **Faiza Ghous D/o Ghous Bux** is accepted in its present form by the Department of Earth Sciences, Quaid-i-Azam University Islamabad as satisfying the requirement for the award of degree of Mphil. Geophysics.

RECOMMENDED BY

Dissertation Supervisor:
Dr. Tahir Azeem ----------

Chairperson of the Department:
Dr. Aamir Ali ----------

External Examiner: ----------

Dedication

I am thankful for all of those who said NO to me. It's because of them I'm doing it myself.

ACKNOWLEDGEMENT

This thesis becomes a reality with the kind support and help of few individuals. I would like to extend my sincere thanks to all of them. Foremost, I want to offer this endeavor to our **Allah Almighty** for the wisdom he bestowed upon me, the strength, peace of my mind and good health in order to finish this research.

I am especially grateful to my honourable supervisor **Dr. Tahir Azeem** for giving me an initiative to this study as well as for providing necessary information regarding the research. I am also thankful to **Dr. Shahid Riaz** for supporting me in my thesis, specially Thanks for your kind guidance, sharing valuable knowledge and technical know-how during the research.

I specially acknowledge the prayers, endless love, efforts and support of my whole family (especially my parents **Perveen Akhter** and **Ghous Bux**), my siblings**,** my friend **Rukshinda** for always being my side. Last but not the least I would also like to thank **Abubakr** for existing during this journey.

FAIZA GHOUS

(March 2022)

ABSTRACT

The study area extends 1200 kilometers in Northern Pakistan, located in the Central Himalayas. This region includes major faulting of MBT, MCT, MKT, MMT and other faults. This region has been the site of numerous devastating earthquakes. So far, very few studies have been conducted to determine earthquake/fault interaction and hazard assessment of this region. The aim of this research is to understand the static earthquake stress triggering in Central Himalayas Pakistan region. For this, historical/instrumental earthquake catalogues were compiled to choose the major earthquakes, having magnitude ≥6.0. The final earthquake sequence comprised of twelve earthquakes, spanning from 1905 to 2005.

By employing static earthquake triggering theory on the final earthquake sequence, we have calculated co-seismic stress changes caused by particular earthquake as well as the impact of earthquakes on the impending earthquakes by incorporating the visco-elastic relaxation. To verify the robustness of numerical results, various values for co-efficient of friction (0.2, 0.4 and 0.6) and various values of viscosities such as (1.0×10^{19} and 1.0×10^{20} Pa.s) were chosen for the lower crust and the upper mantle. Further, the areas that are in high CFS zones and have potential to trigger upcoming earthquakes were analyzed.

Out of twelve earthquakes the one earthquake is caused by previous earthquake. That earthquake is the Aftershock of 2005 Kashmir earthquake having magnitude of 6.4Mw is occurred in high CFS lobe. This earthquake was triggered by the co-seismic CFS changes caused by the 2005 earthquake (Main shock). This is the only time-dependent earthquake in this sequence which has been triggered by a preceding earthquake. The remaining eleven earthquakes in the sequence are all independent. Results reveal that the role of earthquake triggering is ineffective in this study area. Therefore, it can be deduced that the cause of earthquakes in this region is tectonic loading rather than stress transfer. This study will improve the knowledge of earthquake triggering as well as fault interaction in the study area.

TABLE OF CONTENT

TABLE OF FIGURES

LIST OF TABLES

LIST OF GRAPHS

CHAPTER 01

INTRODUCTION

1.1 Overview

Many natural and anthropogenic catastrophes have shaken mankind. Natural disasters i.e., an eruption of volcanoes, flood cyclones, drought, forest fires, earthquakes, and epidemics are well-known in different parts of our planet. The major contributors in natural disasters include earthquake events that result in loss of life, socioeconomic disorder as well as the destruction of property. Over the years, these losses have developed due to an increase in material resources and an increase in population. The most powerful earthquakes have been known to cause massive damage and wipe out entire societies and civilizations (Ambraseys & Douglas, 2004).

An earthquake is a ground vibration or shaking generated by the slipping and rupturing of a fault inside the crust. The energy trapped in compressed rocks releases abruptly because of ruptures or quick slides along fault lines. The energy can be accumulated for a long time in the rocks before being released in seconds. More elastic energy is stored in rocks due to strain on the rocks, which increases the likelihood of an earthquake occurrence. An earthquake's abrupt release of energy creates low-frequency acoustic signals known as seismic waves which move along the surface or within the earth's crust (Barka,1999).

Quite apart from the danger posed by an earthquake, it can also trigger several other natural disasters. The energy released by earthquakes can readily cause slope failures. A tsunami may form, causing coastal regions to be flooding. These occurrences occur in conjunction with volcanic activity, posing an additional risk (Glasser, 2020).

Pakistan is located in one of the most seismically active zones in the world, where the north-west moving Indian plate collides with the south-east moving Eurasian plate at a pace of around 1.7 inches per year (4.3 cm/yr.). The region is experiencing strong seismic activity as a result of the continental-continental collision.

Many mountain systems were formed as a result of this collision, including the Hindukush mountains, the Pamir ranges, the Kirthar and Sulaiman ranges, and the Karakorum mountains. The slip of the major faults caused by this collision resulted in large, frequently devastating earthquakes (Sultan, 2015). The following are some examples of disastrous earthquakes:

1. On October 8, 2005, a tremendous earthquake of magnitude 7.5 hits Kashmir, Pakistan, killing approximately 80,000 people and rendering 5 million people homeless.
2. Another earthquake of magnitude 6.4 happened on October 29, 2008, in Quetta, Pakistan, killing over 10,000 people and rendering 0.5 million people homeless.
3. Great 2013 Awaran Earthquake of magnitude 7.7 killed over 825 people.

1.2 Static Earthquake Triggering

The stress changes are associated with an earthquake define the earthquake triggering mechanism, which can stimulate or retard seismic activity in local areas or trigger future earthquakes at longer distances. This process results from the shifting of stresses caused by an earthquake. However, the earthquake's overall function is to alleviate the elastic stress collected in the crust, where these stresses are enhanced occurs as a result of coseismic fault slip (Freed, 2005). Earthquakes are induced by stress fluctuations of 0.01 MPa, which are sufficient to cause seismicity.

Static triggering may be utilized for a variety of investigations, such as co-seismic, seismic hazard, earthquake triggering (major inter-event), and so on. Seismic Hazard Assessment is a method used by geophysicists to evaluate earthquakes and their related uncertainty. Natural or man-made phenomena, such as earthquakes or hurricanes, have distinct locations in time and space (Wang, 2011).

Seismological and geological investigations give detailed information on earthquakes and their properties. Static earthquake triggering is a useful method for researching the link between earthquakes and, as a consequence, assessing the seismic hazard in a given location. This approach is applied to the research region, which included calculating earthquake stresses due to static earthquake triggering and then

developing stress maps, which assisted us in delineating sensitive zones that are relevant for hazard assessment.

1.3 Coulombs Failure Stress

In seismology, the Coulomb-stress theory plays an important role in understanding how earthquakes trigger each other. Earthquakes create stress fields around their vicinity, the field may be positive or negative depending on the nature of the earthquake (Navas-Portella et al., 2022). The effects of major earthquakes on Coulomb failure stress (CFS) and their relationship with triggering other related earthquakes has been a hot topic of discussion in the past few decades (e.g., Harris, 1998, Stein, 1999, Steacy et al., 2005, Gomberg & Felzer, 2008). Following significant earthquakes, periodic studies reveal changes in tectonic loading in the area and on the fault, allowing for the evaluation of the region's post-seismic earthquake potential.

Our basic knowledge of earthquake physics is that pressure builds up in certain areas due to various reasons and that those areas rupture when the tension exceeds the material's strength. The earthquake is the result of that surpassing the threshold. Stresses can fluctuate through a variety of sources, including tectonic forcing as well as previous earthquakes. As a result, monitoring such changes in the stress field is important for anticipating seismic and volcanic hazards and recommending appropriate strategies to mitigate them. (Stein et al., 1992).

1.4 Location of the Study Area

This study was carried out in Central Himalaya in the Pakistan region, a mountainous region situated in the North of Pakistan. The area contains active seismicity and major faulting system. The coordinates of the study area lies between (32-38°N and 68-78°E) as shown in Figure 1.1. It covers an area of 1200 square kilometers.

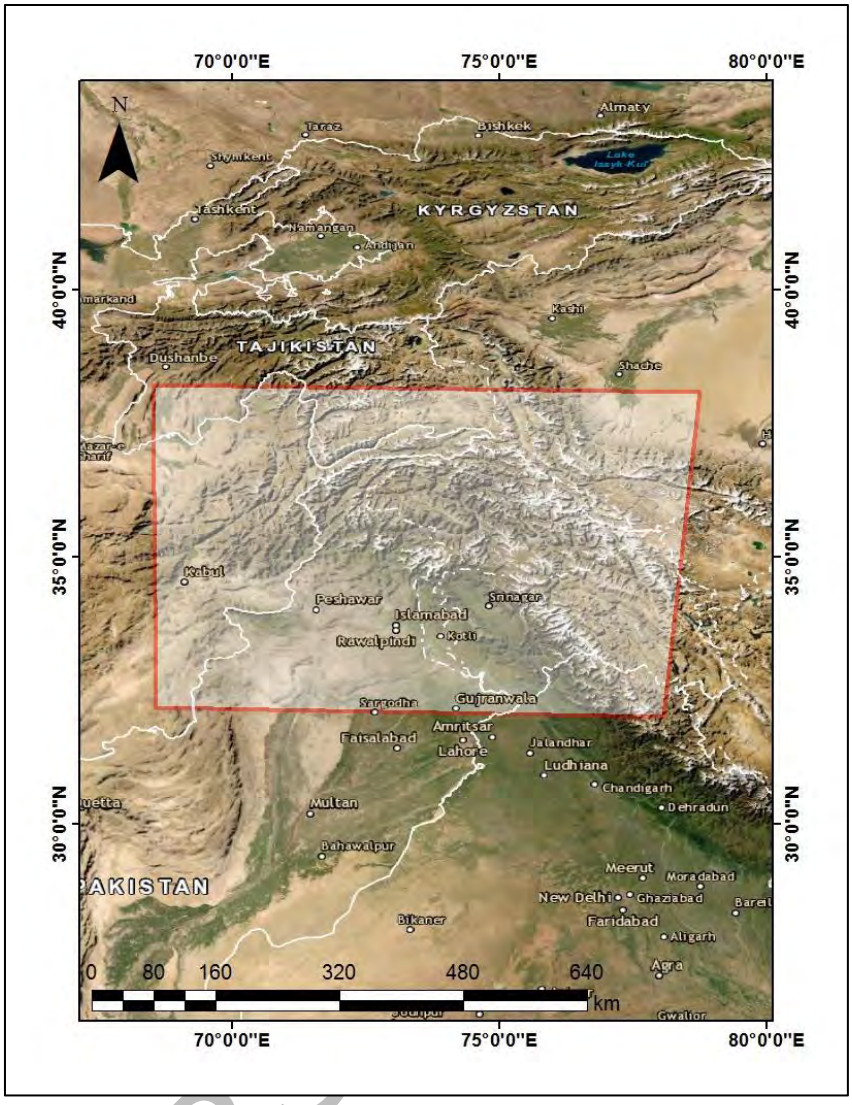

Figure 1.1 Location Map of the study area which is marked by red outline (32-38) N and (68-78) E, which is covering the Northern Pakistan.

1.5 Objective of the Research

The main purpose of this research is to quantify the stress in the study area as well as the seismic hazard in the same region. Furthermore, the results of our proposed study will be useful in better preparing hazard mitigation measures for vulnerable regions. The proposed research's aims are as follows:

1. Find out the focal mechanism solutions of earthquakes to calculate the rupture length, width and uniform slip.
2. Calculate the Coulomb stresses from static earthquake triggering and generation of stress maps of the study area.
3. Analyze the Co- seismic and post-seismic stress changes of earthquakes.

4. Identify the seismically vulnerable areas for triggering based on stress transferring.

1.6 Data set and Methodology

For this purpose, several international and national databases were accessed for collecting the historical and instrumentally recorded earthquake events occurred in the study region. Data for the earthquake catalogue was gathered from the PMD, CES, CMT, USGS, SCARDEC, and previously published works. The data-set requires the following parameters:

i. The seismic event's date and timing of occurrence.
ii. The earthquake's longitude and latitude.
iii. The earthquake's magnitude and depth.
iv. The fault's strike, dip, and rake angle of earthquakes.

The steps in the proposed methodology are as follows:

1. Reviewing the previous literature, which will serve as a source of knowledge for the current task, is the first and most important.
2. Then there's the Earthquake catalogue data, which is essential since it gives complete records of contemporary and past seismicity.
3. The next step is to analyze the earthquake catalogue and pre-process the data, which comprises data sources and region-by-region assessment of earthquake events and their related parameters
4. The next phase is stress computation, which comprises several models and methodologies as described in the workflow below (Figure 1.2)
5. Seismic hazard analysis is the next step, which comprises numerical results and analysis, as well as the reliability of numerical data.
6. After that, we'll identify the areas that are particularly stressed and so vulnerable to dangers.

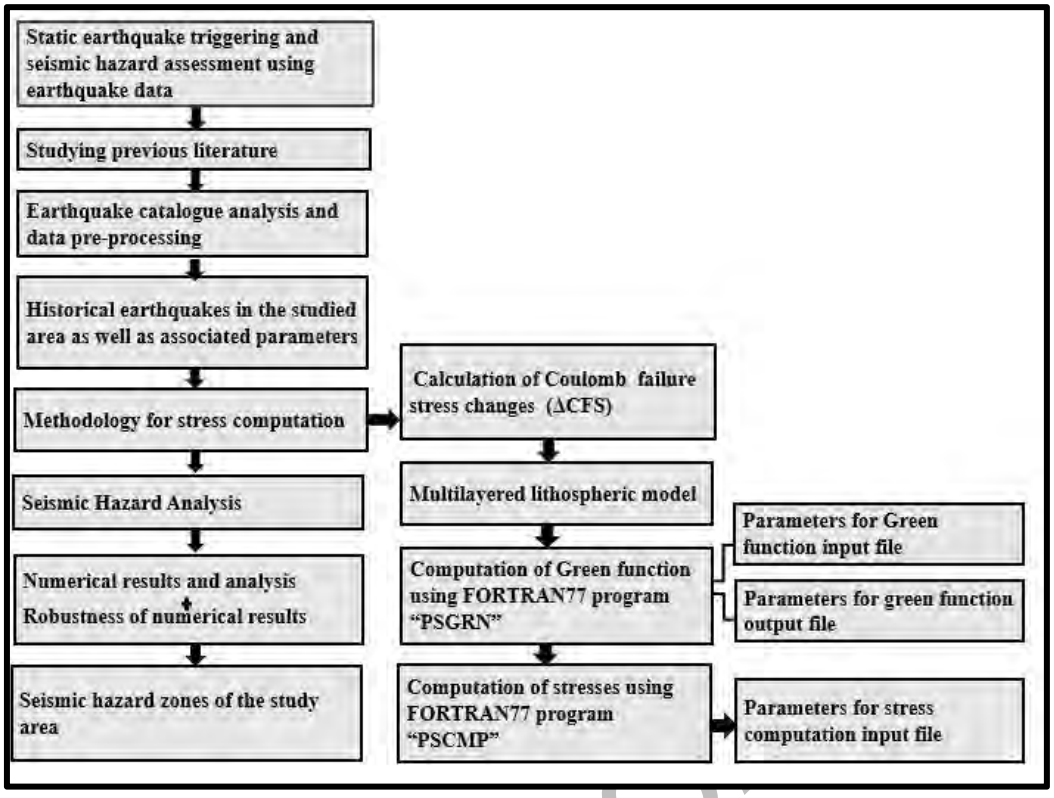

Figure 1.2 Workflow adopted for the computation of Coulomb Stress failure.

CHAPTER 02

GEOLOGY, TECTONICS AND SEISMICIY OF THE HIMALAYAS

2.1 Geological Overview of the Himalayas

2.1.1 Indian and Eurasian collision

Gondwana, a supercontinent in the southern hemisphere was present about 500 million years ago. India was bordered on the west by Madagascar-Africa and on the east by Antarctica within Gondwana. The Paleo-Tethys Ocean ran along Gondwana's northern edge. A sequence of continental chunks migrated away from Gondwana during the Permian, allowing the Neo-Tethys Ocean to follow in their footsteps. In the later Jurassic time, India and Madagascar were drifted away from Africa; later, at around 135 Ma, India was split from East Antarctica and started its northern trip across the Neo-Tethys Ocean, just as the Indian Ocean began forming behind India. The Neo-Tethys ocean floor began to subduct beneath Asia's southern coast as India moved northward (Sorkhabi, 2010).

The Kohistan-Ladakh island bumped into the Karakoram edge around 85 Ma, when the sea bottom between them subducted and closed. At the start, the northwest edge of the Indian plate made contact with Asian plate, possibly as early as 55 Ma or as late as 60-65 Ma, after that, the Neo-Tethys ocean floor closed, and India rotated counterclockwise till the northeastern edge of it docked with Asia at around 45 Ma. The border of this plate collision is marked by the Indus-Tsangpo Suture Zone. This collision led to Himalayan orogeny forming the mountain ranges that we have today. The geology and geography of the Himalayas is given below in Figure2.1.

2.1.2 Division of Himalayan Ranges

The Himalaya are 2400km long and around 300 km wide mountain arc present the southern part of Tibetan Plateau. The Himalayas are the world's highest yet rising highlands. The Tibetan Plateau and its adjacent mountains make up the world's

greatest topographical peak. This region of the world contains all of the mountain peaks higher than 7000 metres, and several huge rivers that originate in these highlands give water to billions of people in Asia (Sorkhabi, 2010).

Geologists have divided the Himalaya into six primary zones based on geological mapping in several regions of the Himalaya. From 110 to 40 million years ago, granitic and volcanic rocks produced the Trans-Himalaya (Ma). The metamorphosed and rocks of Tibetan blocks in south got igneous intrusions. The borderline between the two plates is marked by the Indus-Tsangpo Suture Zone which is the second geological zone of Himalayas. The Tethyan or Tibetan Himalayan zone is made up of sediments from the Cambrian to the Eocene periods that were formed on the Tethys Ocean's continental shelf. Sedimentary rocks in this zone have a stratigraphic width of up to 12 km. The core of the Himalayan Mountain range, the Higher Himalaya, a made of granite and metamorphic rocks with thickness of around 20km (Hodges, 2000).

The Lesser Himalaya is present at south of the Higher Himalaya and is made up of metamorphosed sedimentary rocks of Proterozoic and Cambrian periods. The rock column in this region is 10-20 km broad stratigraphically. Geographically, the Sub-Himalaya also called Siwalik range has elevations ranging from 250 to 800 meters. This zone is composed of a 10-kilometer-thick sequence of sandstone and mudstone that has been brought and deposited by streams from the Himalayan ranges (Sorkhabi, 2010).

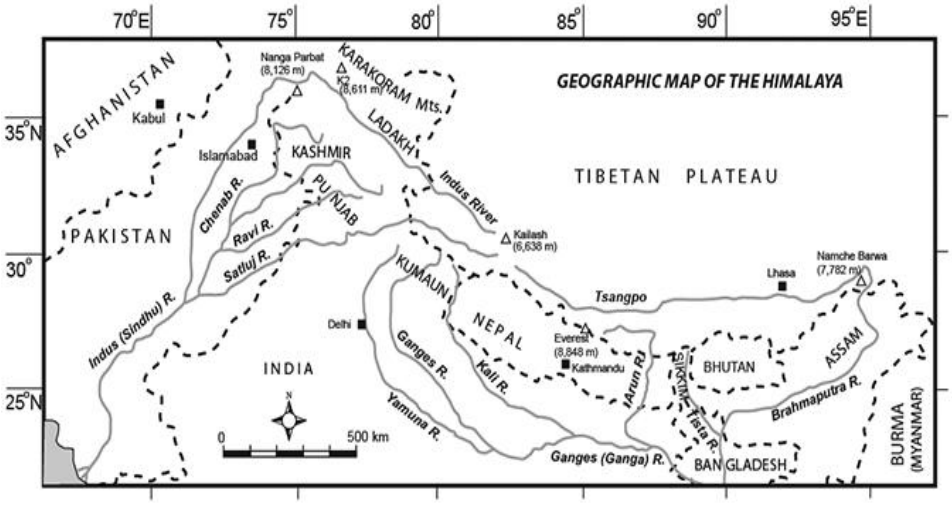

Figure 2.1 Geology and Geographic Map of Himalayas with main boundaries (Sorkhabi, 2010).

2.1.3 The Geology of Himalayas in Pakistan

The syntaxial bend of the Himalayas dominates northern Pakistan's structural characteristics, which are linked to the convergence of the Hindukush and Karakorum ranges. With a cast of NW-SE, the Kashmir Himalayas are most likely manifestations of the main boundary thrust, which can be seen extending eastward in the Himalayan front (Armbruster et al, 1978). At around 73.5E, the Murree thrust, which divides the tertiary Murree formation from the beneath carboniferous Panjal formation, and the Panjal thrust, which distinguishes the carboniferous rocks from the above Precambrian Salkhalla formation, both curves sharply around syntaxis, which can be seen in Figure 2.2.

The western Himalayan syntaxis can be seen in the patterns of most elements in northern Pakistan. Lower crustal seismicity, on the other hand, does not show this pattern. For example, The Pattan earthquake happened in the Indus Kohistan Seismic Zone (IKSZ) (Armbruster et al., 1977), which is a parallel northwest-southeast extension of Panjal and Murree thrust and Main boundary thrust (Armbruster et al., 1978). Since the development of the Tarbela seismicity network, microseismicity at depths more than 12km has been observed, resulting in the formation of the IKSZ.

2.2 Tectonic Setting of Himalayas

The Himalayan was formed as a result of orogeny when the Indian plate collided with Eurasian plates 50-55 million years ago. The Indian plate has spreading centers to the southwest, continental collision boundary to the north, and at east and west, it has transformed boundaries. The absence of volcanoes and significant seismicity is a critical component of the northern collision. Tectonics of this region with major faulting is given below in Figure2.2.

The Northwest Himalayan fold-and-thrust belt spans the long irregularly shaped mountainous region stretching from the Afghan border near Parachinar to the Kashmir Basin. Its eastern border is formed by the Hazara-Kashmir and Nanga Parbat Syntaxes. It encompasses the entire terrain between the Main Mantle Thrust (MMT) in the north and the Salt Range Thrust (SRT) in the south. This region comprises of the Nanga Parbat mountain ranges. Hazara, Swat, Margalla, Kalachitta, KohaL Sufaid Koh, Salt Range, and its western extension (Kazmi & Jan, 1997). The Panjal-

Khairabad Fault, a major thrust fault, divides the NW Himalayan sequence into a deformed southern zone known as the external or foreland zone and a deformed and metamorphosed northern zone known as the hinterland zone (Treloar et al., 2000). The Hazara-Kashmir Syntaxis, Salt Range, and Kohat-Potwar fold belts, as well as the Kurram-Cherat-Margalla thrust belt, make up the foreland zone, while the Himalayan crystalline nappe-and-thrust belt makes up the hinterland zone.

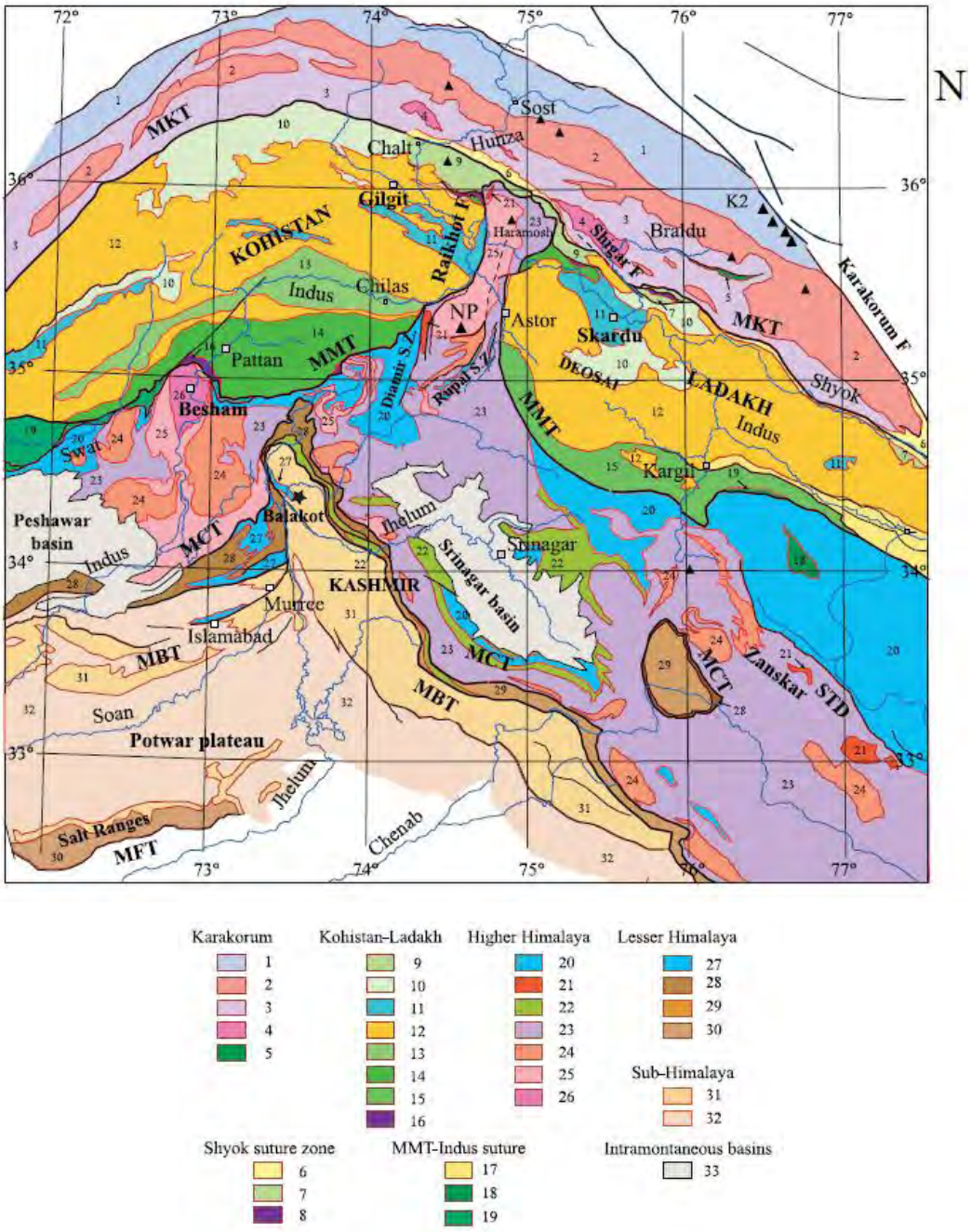

Figure 2.2 Tectonic Map of the NW Pakistan Himalayas with major faulting and main tectonic boundaries: MKT, MMT, MCT and MBT (Pecher et al., 2008).

2.3 Seismotectonics of Himalayas

The earthquake's tragic human and economic consequences have had a significant impact on our knowledge of seismic danger in the western Himalayas. The Himalayan rocks are composed of material that has been part of the Indian subcontinent since its formation, cementation, and renewal. Strike-slip movement, shear faulting, E-W compression, and reverse block movement appear to have generated the geological features. According to (Seeber & Armbruster 1979), the Kangra earthquake of 1905 ripped open an area of 280 x 100 km^2. When combined with the sourced earthquake rupture areas of 1897, 1934, 1950, and 2005 earthquakes, shows that these big earthquakes ruptured more than 50 percent of the Himalayan arc's 2000 km length.

Earthquakes strike Pakistan and its neighboring nations frequently, with some causing significant death and property destruction. Apart from the two existing fold-and-thrust belts of Sulaiman and the northwest Himalaya, strong seismicity zones can be found throughout the country (MonaLisa et al., 2007). According to data available (e.g., Kazmi and Jan 1997), the Makran coastal earthquake having 8.3MS that occurred in 1945, was Pakistan's most severe earthquake. This occurrence resulted in the formation of a handful of offshore islands all along the coast. Activation of MBT happened in 1905 due to the Kangra earthquake with a magnitude of 7.7Mw, MBT is a regional fault that extends to the east of the study area. Recent earthquakes in the research area include those in Pattan (1974), Rawalpindi (1977), Bunji (2002), and Batgram (2004). Following is a description of historical and instrumental seismicity, as well as the seismicity trend seen in the given Figure 2.3 of area in which we can see that this region is prone in seismicity.

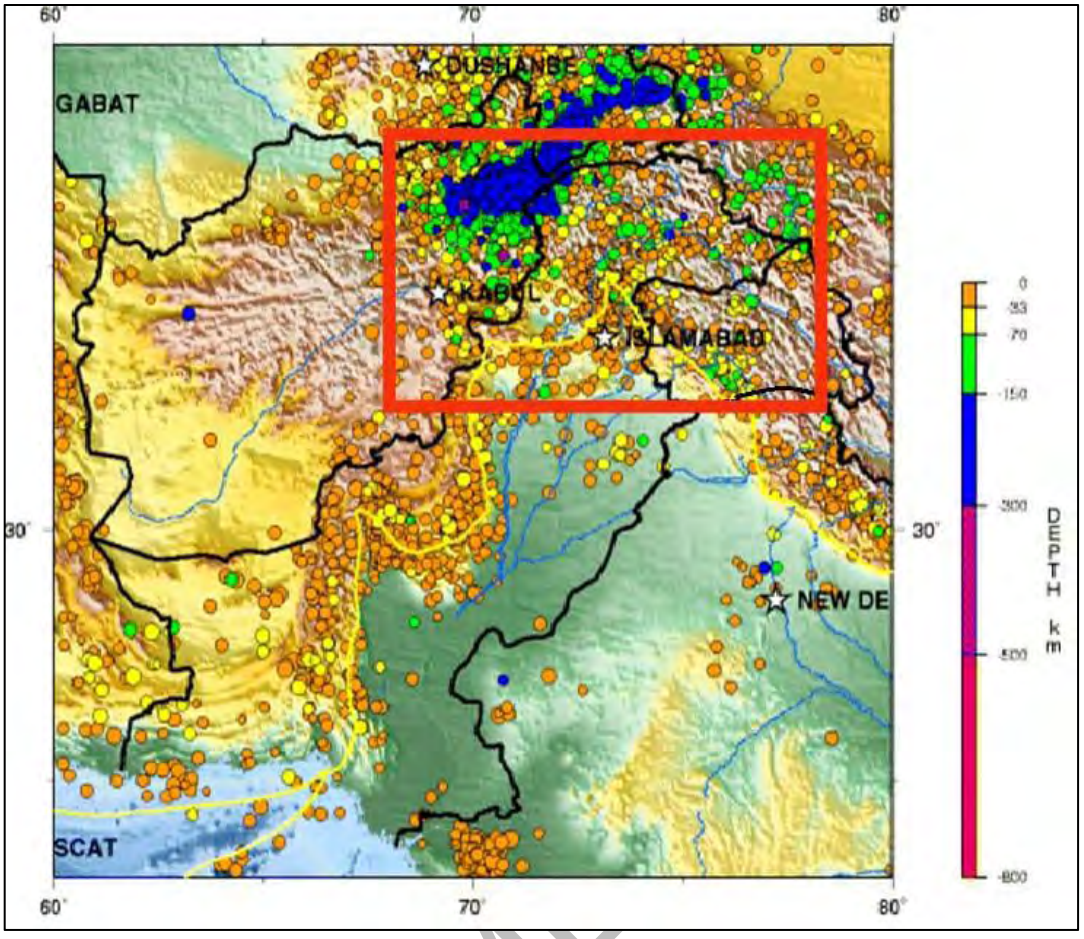

Figure 2.3 Seismicity Map of Pakistan, highlighted zone is showing the study area which is prone in seismicity. (https://seismic.pmd.gov.pk/seismicnew/Seismicity.jpg)

2.3.1 Historical Seismicity

Long before seismic sensors, the destructive power of earthquakes was observed, described, and even recorded in written reports. This data has proven beneficial in not only identifying earthquake-prone places from past times but also aids in finding the probability of life and estimates probable damage. The practice of using intensity scales such as the Modified Mercalli Intensity scale (MMI) to measure this data has aided in assigning differing magnitudes to chronological events in the vicinity of the area. As a result, the seismicity map of the area contains historical data as well.

Considering the above discussion, a variety of catalogues for the study area that include historical seismicity are accessible, as presented in Pakistan Meteorological Department Research report and Centre of Earthquake studies.

2.3.2 Instrumental Seismicity

Even though instrumental earthquake monitoring began in 1904, the quality work regarding earthquake detection and localization improved in 1964 when the worldwide seismographic sites network (WWSSN) covered the subcontinent, which included approximately 120 stations in 60 nations where the Pakistan contains five of these stations shown in Figure 2.4. As a result, statistics from 1904 to 1964 in the region are severely limited. Current seismicity is reported by the International Seismological Summary (ISS), Worldwide Standard Seismograph Network (WWSSN), the United States Geological Survey (USGS), the International Seismological Centre (ISC), Center of Earthquake Studies (CES), and the Pakistan Meteorological Department.

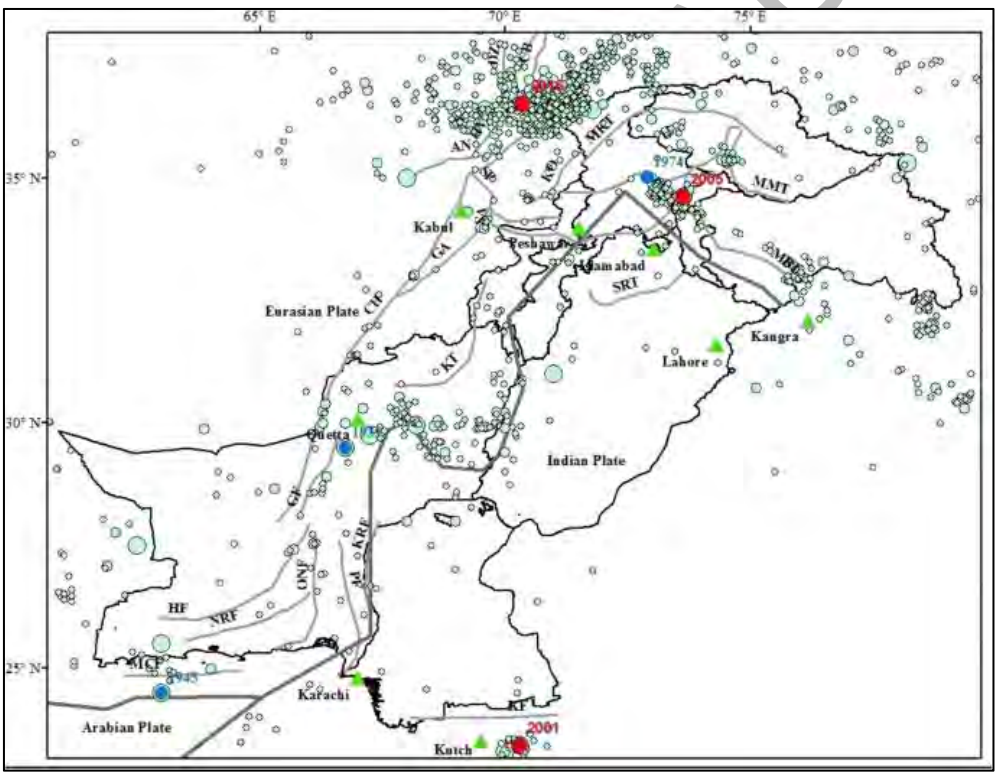

Figure 2.4 Seismicity Map of Pakistan along with 5 observatory stations all over the country in green rectangles, where red circles are showing devastating earthquakes and thick black lines indicating the location of boundaries (Rehman, & Burton 2020).

CHAPTER 03

EARTHQUAKE CATALOGUE ANALYSIS AND DATA PROCESSING

3.1 Introduction

Earthquake catalogues are the primary sources of data for the current hazard assessment. For accurate stress computations and seismic hazard assessments, a complete earthquake catalogue is required. The longer the catalogue is, the more accurate the parameters are and the more valuable it is for calculating earthquake risk (Kagan, 1991).

3.2 Data sources

Data from earthquake catalogues is essential because it provides a systematic record of contemporary and historical seismic activity. Data for the earthquake catalogue was obtained from a variety of sources, including previously published publications and catalogues established by various national and international organizations such CES, USGS, ISC, and others. The following are the key catalogues that were used as a foundation for this study:

1. Pakistan Meteorological Department (PMD).
2. National Centre of Earthquake Studies Pakistan (CES).
3. National Earthquake Information Center, United States Geological Survey (USGS) (NEIC).
4. The CMT catalogue (Harvard Centroid Moment Tensor Project, 2009).
5. Database of the International Seismological Centre England (ISC).
6. SCARDEC Source Time Functions Database.

3.3 Selected Earthquakes for Analysis

In this study, a simplified earthquake catalogue is generated by modifying the above-mentioned catalogue for the study area, bearing in mind the study's objectives.

Both published and online earthquake databases were thoroughly examined (Ambraseys & Bilham, 2003). With the help of the above-mentioned data sources, a new catalogue file for the research region is generated. More than a hundred earthquakes with magnitudes (Mw) ranging from (5.0 to 9.5) are included in the basic collected catalogue. The final catalogue file, which includes 12 earthquakes with magnitudes ranging from (6.0 to 8.0)Mw and depth ranging from (5 to 30)km, is created from these earthquakes. We only selected these earthquakes with magnitudes ranging from (6.0 to 8.0)Mw because earthquakes with M<6.0 have a negligible CFS impact. List of selected earthquakes with particular date, location, Magnitude and depth is given below in table 3.1, and the graphical representation of the earthquakes with depth and magnitude is also given in graph 3.1.

No. of Events	Years	Months	Date	Lat	Long	Magnitude (Mw)	Depth (km)
1	1905	4	4	33.0	76.15	7.7	20
2	1972	9	3	36.12	73.42	6.2	30
3	1981	9	12	35.32	73.48	6.1	10
4	1982	12	16	36.40	68.75	6.4	12
5	1984	2	1	35.59	70.50	6.1	25
6	1990	3	5	36.87	73.00	6.1	20
7	1992	5	20	32.95	71.27	6.0	15
8	1996	11	19	35.45	77.86	6.8	15
9	1998	5	30	37.70	70.45	6.6	30
10	2002	11	20	35.40	74.64	6.3	15
11	2005	10	8	34.43	73.64	7.5	8
12	2005	10	8	34.94	73.10	6.4	12

Table 3.1 List of selected Earthquakes with date, location, Magnitude, and depth.

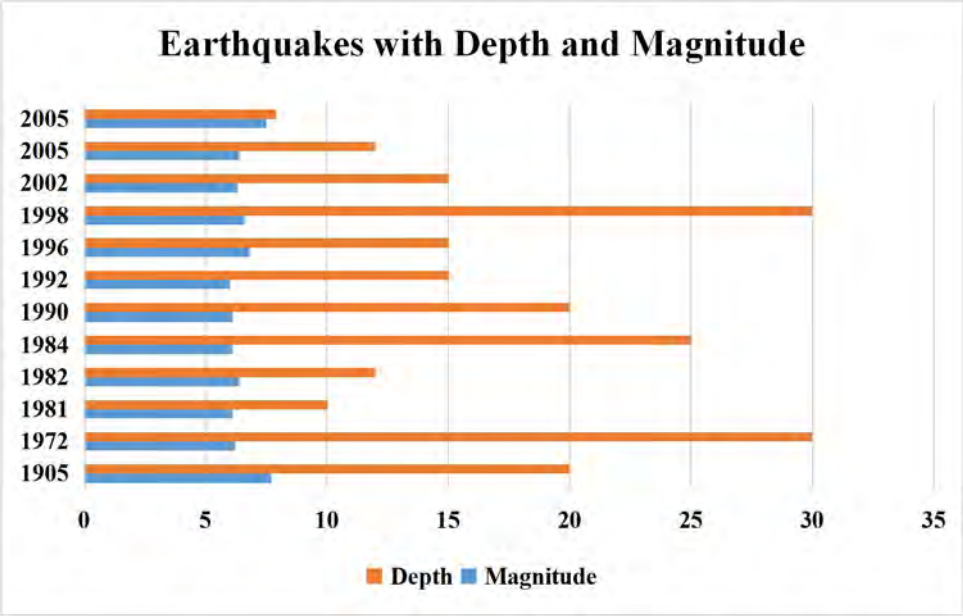

Graph 3.1 Graphical representation of selected earthquakes with depth and magnitude.

3.4 Focal Mechanism Solutions of the Selected Earthquakes

An earthquake's focal mechanism shows the direction of slip in an earthquake as well as the orientation of a fault on which it appears. So we also considered the earthquake's focal mechanism, which includes the strike, dip, and rake angle associated with the fault. The focal mechanism of all selected earthquakes are given below in table 3.2.

No. of Events	Year	Month	Date	Lat	Long	Magnitude (Mw)	Depth (km)	Strike	Dip	Rake
1	1905	4	4	33.0	76.15	7.7	20	85°	5°	110°
2	1972	9	3	36.12	73.42	6.2	30	270°	29°	125°
3	1981	9	12	35.32	73.48	6.1	10	107°	36°	79°
4	1982	12	16	36.40	68.75	6.4	12	218°	43°	114°
5	1984	2	1	35.59	70.50	6.1	25	268°	37°	121°
6	1990	3	5	36.87	73.0	6.1	20	192°	36°	-46°
7	1992	5	20	32.95	71.27	6.0	15	237°	5°	79°
8	1996	11	19	35.45	77.86	6.8	15	180°	71°	170°
9	1998	5	30	37.70	70.45	6.6	30	111°	85°	175°

10	2002	11	20	35.40	74.64	6.3	15	209°	42°	-107°
11	2005	10	8	34.43	73.64	7.5	8	331°	29°	125°
12	2005	10	8	34.94	73.10	6.4	12	328°	39°	107°

Table 3.2 Focal mechanism of selected earthquakes (Strike, Dip and Rake).

At the end of above findings of earthquake's focal mechanism and all other parameters, we plotted them on our study area map to find out the nature of earthquakes as well as their location in the study area. So, Figure3.1 is showing the focal mechanism of earthquakes in the study area with their particular location.

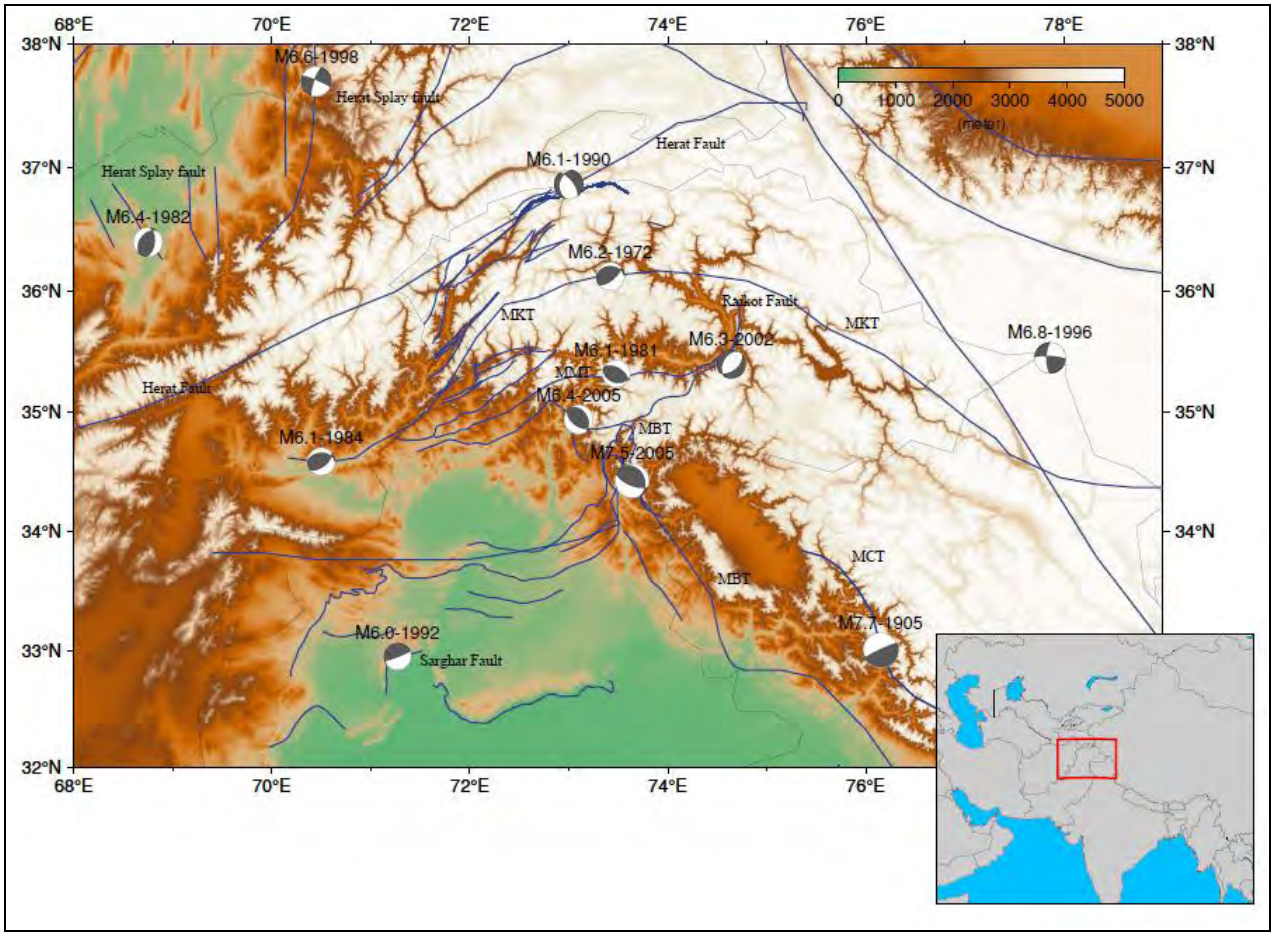

Figure 3.1 Location Map of all the earthquakes with their focal mechanism solution in the area with major faulting.

The beach balls on the study area map are the representation of earthquake nature. The plotting of these beach balls is based on the focal mechanism solutions of each earthquake. Blue lines on this map is showing the major faulting in the area. The Map is showing the Thrust faulting in the area the earthquakes which are thrust, Strike-slip,

and Normal dip-slip in nature. As we can see on the map the 1905 earthquake is purely a strike-slip earthquake which was occurred on the MCT fault. The 1972 and 1984 earthquakes were thrust in nature and both have occurred on MKT. The 1990 earthquake which is a Normal dip-slip in nature was occurred on the Herat fault, while the 1982 earthquake which is thrust in nature, and 1998 which is a Normal dip-slip in nature both have occurred on Herat fault splays. The 1981 earthquake is Thrust in nature which was occurred on MMT. The 1992 earthquake which is strike-slip in nature was occurred on the Sarghar fault. The 1996 earthquake is Normal in nature with Strike-slip component. The 2002 earthquake which is a Normal Dip-slip in nature occurred on the Raikot fault, this earthquake is normal in nature due to gravity collapse in this specific region. The main earthquake (Kashmir 2005) and its aftershock both are thrust in nature which was occurred on MBT.

3.5 Earthquake Parameters Calculation using Empirical relation

The maximum and uniform displacement/slip per event, as well as the moment magnitude, surface rupture length, subsurface rupture length, downdip rupture width as well as rupture area, are all calculated using historical earthquake parameters from all over the world. (Well & Coppersmith, 1994).

If we know the magnitude of the earthquake, we may use the scaling relation to determine the length of the rupture, width of rupture, and uniform slip of that particular earthquake, and vice versa. We estimated the rupture width, rupture length, and uniform slip for all the selected earthquakes in the final catalogue using the equations (Well & Coppersmith, 1994), which are listed in table 3.3, for strike slip, reverse, and normal faults.

Empirical relation source parameters	**Equation**	**Slip Type**	**Co-efficients and standard errors**	
			a	**b**
Rupture length	**log(SRL) =a + b*M**	Strike-slip(SS)	-3.55	0.74
		Reverse (R)	-2.86	0.63
		Normal (N)	-2.01	0.5

Rupture width	**log(RW) = a + b*M**	Strike-slip(SS)	-0.76	0.27
		Reverse (R)	-1.61	0.41
		Normal (N)	-1.14	0.35
uniform displacement/slip	**log(AD) =a + b * M**	Strike-slip(SS)	-6.32	0.90
		Reverse (R)	-0.74	0.08
		Normal (N)	-4.45	0.63

Table 3.3. Earthquake parameters using empirical relation

Using the empirical relationship, we derived the source parameters for the final catalogue from table 3.3, namely rupture length, rupture width, and uniform slip which are listed below in Table 3.4. By using these parameters, we will compute Coulombs failure stresses for the study area. In these given tables we have obtained focal mechanism and other parameters of each earthquake which are not calculated before for this region to compute stress changes. For the event of 2005 main shock we also calculated such parameters, but in literature we have found the rupture model of this event which is about (9 by 9)km^2 in area. The area is divided into 84 patches which is containing fault in each patch. So the area of this rupture model having 84 faults as well. The rupture model of this particular earthquake is giving information about stresses on every point. We have attached the input file(Rupture Model) of this earthquake with all parameters in Appendices portion. According to the given rupture model of 2005 Main shock the strike of the earthquake is 331°, the dip is 29°, and the rake angle is 125.

No. of Events	**Year**	**Month**	**Date**	**Lat**	**Long**	**Mag**	**Rupture length(km)**	**Rupture width(km)**	**Uniform Slip (m)**
1	1905	4	4	33.0	76.15	7.7	97.9	35.2	0.8
2	1972	9	3	36.12	73.42	6.2	11.1	8.6	0.6
3	1981	9	12	35.32	73.48	6.1	9.6	9	0.6
4	1982	12	16	36.40	68.75	6.4	14.9	12	0.6
5	1984	2	1	35.59	70.50	6.1	9.6	9	0.6
6	1990	3	5	36.87	73.0	6.1	9.6	9	0.6
7	1992	5	20	32.95	71.27	6	8.3	7.1	0.5

8	1996	11	19	35.45	77.86	6.8	24.5	17.4	0.7
9	1998	5	30	37.70	70.45	6.6	19.5	14.8	0.5
10	2002	11	20	35.40	74.64	6.3	12.9	9.4	0.6
11	2005	10	8	34.94	73.10	6.4	14.9	10.3	0.6
12	2005	10	8	34.43	73.64	7.5	73.3	29.2	0.7

Table 3.4 Final earthquake catalogue along with other calculated source parameters.

3.6 Graphical Representation of Earthquakes

At the end of all the required calculations of earthquake parameters, we plotted them to check the effect of magnitude on the rupture length, width and slip. As the rate magnitude increases the rupture length and width also increases which can be seen in individual and combined graphs which are given below. Graph 3.2, 3.3 and 3.4 shows the greater the magnitude the greater its rupture length and width. The slip is not incorporated here because slip is mostly dependent on the earthquake type/nature, which we have seen in Figure3.1.

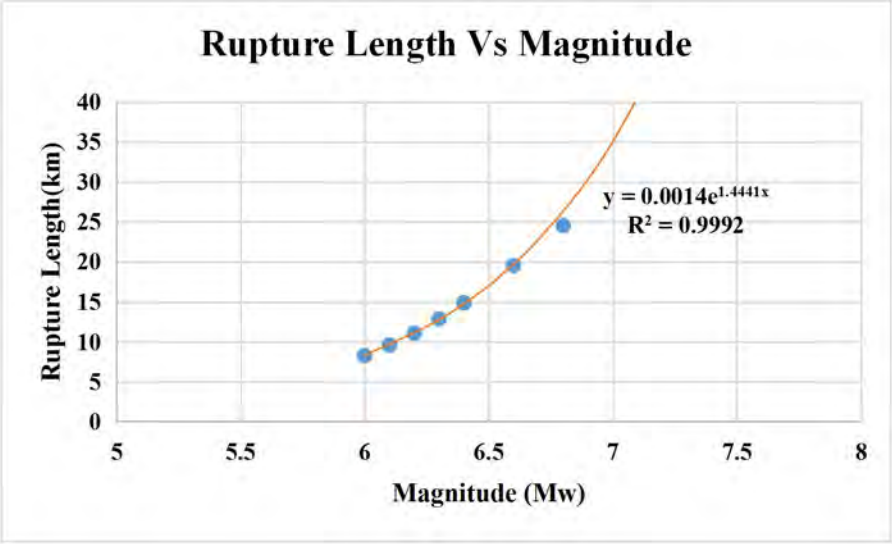

Graph 3.2 Magnitude of the earthquakes and their Rupture length. Trend line is showing the exponential relation between Rupture length and magnitude.

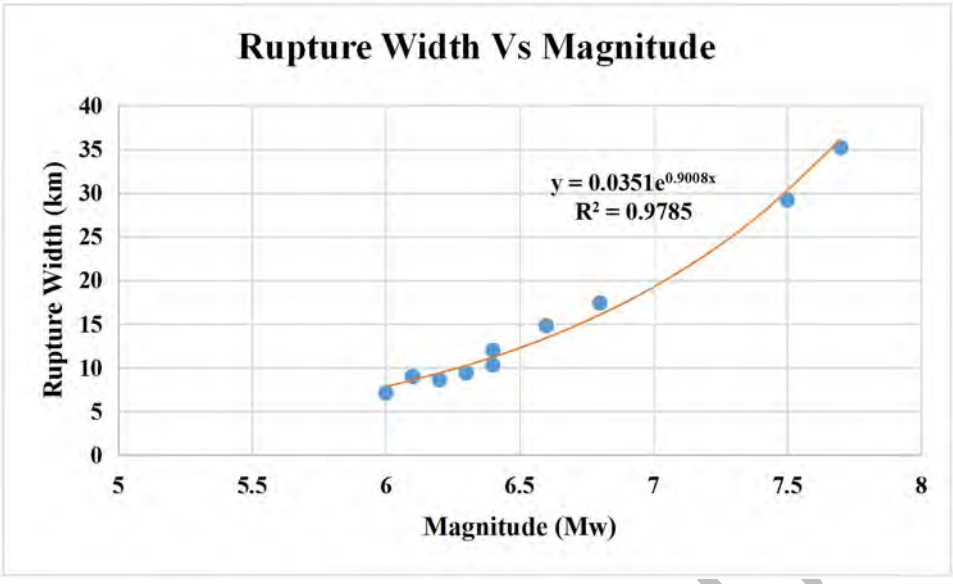

Graph 3.3 Magnitude of the earthquakes and their Rupture Width. Trend line is showing the exponential relation between Rupture width and magnitude.

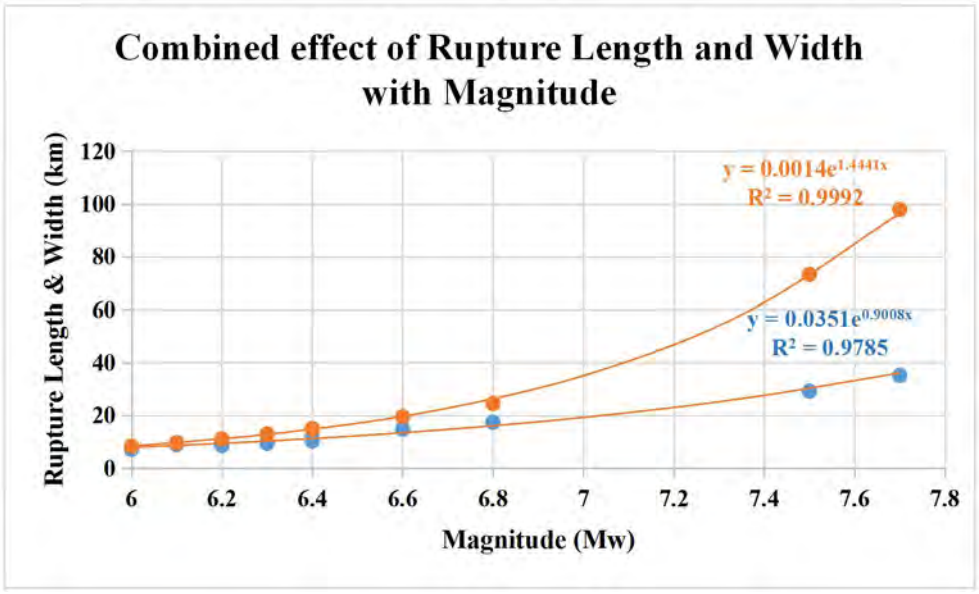

Graph 3.4 Magnitude of the earthquakes with combined effect of their Rupture Length and Width.

The individual and combined effect of rupture length and width with magnitude is showing the exponential relation between them. Exponential relation can be seen by the trend line and equation as well. Hence, the magnitude of the earthquake increases the rupture length and the width also increases while the slip of the earthquake depends on the nature of the earthquake type.

3.7 Discussion of the selected Earthquakes

3.7.1 The 1905 Earthquake (M= 7.7)

The 1905 earthquake occurred on 4 April 1905, with the magnitude of 7.7Mw. The epicentre of the earthquake was 33.0°N 76.15°E with the depth of 20km. From the Focal mechanism solutions in Table 3.1 and Figure 3.1, the earthquake parameters are Strike=85°, dip=5°, and rake angle=110°. This earthquake is strike-slip in nature which was occurred on MCT fault. This earthquake was one of the most devastating in Himalaya.

3.7.2 The 1972 Earthquake (M= 6.2)

The earthquake occurred on 3 September 1972, with the magnitude of 6.2 Mw. The epicentre of this earthquake was 36.12°N and 73.42°E, with the depth of 30km. From the Focal mechanism solutions in Table 3.1 and Figure 3.1, the earthquake parameters are Strike=270°, dip=29°, and rake angle=125°. This earthquake is thrust in nature with strike-slip component, which was occurred on MKT fault.

3.7.3 The 1981 Earthquake (M= 6.1)

The earthquake occurred on 12 September 1981, with the magnitude of 6.1 Mw. The epicentre of this earthquake was 35.32°N and 73.48°E, with the depth of 10km. From the Focal mechanism solutions in Table 3.1 and Figure 3.1, the earthquake parameters are Strike=107°, dip=36°, and rake angle=79°. This earthquake is thrust in nature with strike-slip component, which was occurred on MMT fault.

3.7.4 The 1982 Earthquake (M= 6.4)

The earthquake occurred on 16 December 1982, with the magnitude of 6.4 Mw. The epicentre of this earthquake was 36.40°N and 68.75°E, with the depth of 12km. From the Focal mechanism solutions in Table 3.1 and Figure 3.1, the earthquake parameters are Strike=218°, dip=43°, and rake angle=114°. This earthquake is thrust in nature with strike-slip component, which was occurred on Herat fault.

3.7.5 The 1984 Earthquake (M= 6.1)

The earthquake occurred on 1st of February 1984, with the magnitude of 6.1 Mw. The epicentre of this earthquake was 35.459°N and 70.5°E, with the depth of 25km. From the Focal mechanism solutions in Table 3.1 and Figure 3.1, the earthquake parameters are Strike=268°, dip=37°, and rake angle=121°. This earthquake is thrust in nature with strike-slip component, which was occurred on MKT fault.

3.7.6 The 1990 Earthquake (M= 6.1)

The earthquake occurred on 5th of March 1990, with the magnitude of 6.1 Mw. The epicentre of this earthquake was 36.87°N and 73.0°E, with the depth of 20km. From the Focal mechanism solutions in Table 3.1 and Figure 3.1, the earthquake parameters are Strike=192°, dip=36°, and rake angle=-46°. This earthquake is normal in nature with strike-slip component, which was occurred on Herat fault.

3.7.7 The 1992 Earthquake (M= 6.0)

The earthquake occurred on 20 May 1992, with the magnitude of 6.0 Mw. The epicentre of this earthquake was 32.95°N and 71.27°E, with the depth of 15km. From the Focal mechanism solutions in Table 3.1 and Figure 3.1, the earthquake parameters are Strike=237°, dip=5°, and rake angle=79°. This earthquake is strike-slip in nature, which was occurred on Sarghar fault.

3.7.8 The 1996 Earthquake (M= 6.8)

The earthquake occurred on 19 November 1996, with the magnitude of 6.80 Mw. The epicentre of this earthquake was 35.45°N and 77.86°E, with the depth of 15km.

From the Focal mechanism solutions in Table 3.1 and Figure 3.1, the earthquake parameters are Strike=180°, dip=71°, and rake angle=170°. This earthquake is Normal in nature with strike-slip component.

3.7.9 The 1998 Earthquake (M= 6.6)

The earthquake occurred on 30 May 1998, with the magnitude of 6.6 Mw. The epicentre of this earthquake was 37.70°N and 70.45°E, with the depth of 30km. From the Focal mechanism solutions in Table 3.1 and Figure 3.1, the earthquake parameters

are Strike=111°, dip=85°, and rake angle=175°. This earthquake is Normal dip-slip nature, which was occurred on Herat fault.

3.7.10 The 2002 Earthquake (M= 6.3)

The earthquake occurred on 20 November 2002, with the magnitude of 6.3 Mw. The epicentre of this earthquake was 35.40°N and 74.64°E, with the depth of 15km. From the Focal mechanism solutions in Table 3.1 and Figure 3.1, the earthquake parameters are Strike=209°, dip=42°, and rake angle=-170°. This earthquake is Normal dip-slip in nature, which was occurred on Raikot fault.

3.7.11 The 2005 Earthquake (M= 7.5) Main-shock

The earthquake occurred on 8 October 2005, with the magnitude of 7.5 Mw. The epicentre of this earthquake was 34.43°N and 73.64°E, with the depth of 8km. From the Focal mechanism solutions in Table 3.1 and Figure 3.1, the earthquake parameters are Strike=331°, dip=29°, and rake angle=125°. This earthquake is thrust in nature with strike-slip component, which was occurred on MBT fault.

3.7.12 The 2005 Earthquake (M=6.4) Aftershock

The earthquake occurred on 8 October 2005, with the magnitude of 6.4 Mw. The epicentre of this earthquake was 34.94°N and 73.10°E, with the depth of 12km. From the Focal mechanism solutions in Table 3.1 and Figure 3.1, the earthquake parameters are Strike=328°, dip=39°, and rake angle=107°. This earthquake is thrust in nature with strike-slip component, which was occurred on MBT fault.

CHAPTER 04

COULOMB FAILURE STRESSES

4.1 Introduction

The process by which a stress perturbation is interacted to the fault is referred to as "stress transfer." Because the sources of stress changes and the processes of stress transfer vary over spatial and temporal, hazard assessments must account for these variations as well. Understanding as well as quantifying this falls under the purview of "time-dependent seismic hazard." The three primary sources of stress transfer include:

1. Tectonic loading,
2. Static earthquake stress transfer
3. Viscoelastic stress transfer

In this study static earthquake stress transfer and viscoelastic stress transfer will be incorporated while tectonic loading will remain fixed.

4.2 Models and Methods for Computing Coulomb Failure Stress

The model and methods for stress computation have been explained in the following sections:

4.2.1 Calculation of Coulomb Stress Changes

Our study was carried out by determining the change in Coulomb failure stress owing to earthquake using the following expression (Scholz, 1990).

$$\Delta CFS = \Delta\tau + \mu'\Delta\sigma N \quad \text{..... (1)}$$

Where, τ=shear stress, σ = normal stress, μ'= effective co-efficient of friction.

The change in normal and shear stress represents the slip direction for a subsequent event (the receiver), where **ΔσN** is positive for rising clamping normal stress with positive pressure specified. Regional faults which are closer to failure lies in positive ΔCFS zones, whereas faults which are further away from the failure lies in negative ΔCFS zones according to the equation **(1).** (Freed, 2005).

The focal mechanism solution for the earthquakes that were chosen, as well as the earthquake parameters employed in this current study, are stated in Table 3.2. For the determination of co-seismic and post-seismic stresses, we employed a model with dislocation sources enclosed in a layered half space with mixed elastic and inelastic properties. In addition, we used the PSGRN/PSCMP programmes (Wang et al., 2006) to quantify surface and subsurface deformation induced by geophysical sources in a multi - layered viscoelastic gravitational half-space. At last, we estimated the CFS on the earthquaketo use both co-seismic static as well as viscoelastic stress transfer changes since the 1905 earthquake.

In this study, we chose linear Maxwell rheology over a complex rheological model to calculate the viscoelastic effect because viscoelastic relaxation at a timescale of 100 years indicates negligible variations in stress changes (Verdechia & Carena, 2015). Due to the limited amount of geodetic measurements in the study area, we used a reasonable value of 1×10^{19} Pa.s for viscosities of both the lower crust as well as the upper mantle in a simulation performed at 30km depth. The robustness of the numerical results will be investigated further by varying the viscosity values for the lower crust and upper mantle.

4.2.2 Multilayered Viscoelastic Model (Crust 1.0 Model)

A 1D layered structural model (stair-case model) has been utilized for the computation of green function, reported in table 4.1. Due to the lack of local seismic observations and different velocity patterns in the region of interest, we created a reference lithospheric model consisting of upper, middle, and lower crust along with lithospheric mantle based on CRUST 1.0 (https://igppweb.ucsd.edu/gabi/crust1.html). In CRUST 1.0, there will be 10–40 crustal types. Each of the 1x1-degree cells will have its own 8-layer crustal profile consisting of :

1. Water
2. Ice
3. Upper sediments
4. Middle sediments
5. Lower sediments
6. Upper crust
7. Middle crust
8. Lower crust

Seismic studies determine the thickness, density, Vp and Vs of each layer. The shear modulus is calculated using the formula in this equation: (Aki & Richards, 2002).

$$\mu = \rho Vs2 \approx 1/3\ \rho Vp2 \ldots\ldots\ldots\ldots\ldots\ldots\ldots\ldots\ldots\ldots.(2)$$

We selected a moderate value of 0.4 for the co-efficient of friction (μ′) in our simulation (King et al., 1994). Based on the structure (1D velocity model) of our study area for which we want to calculate the stresses, and to analyze to the response of the stresses that how it will behave, computation of green function is necessary. We employed two programs/utilities for the computation of stresses i.e PSGRN and PSCMP codes (Wang et al., 2006), in order to achieve the study's goal PSGRN is used to compute the green function of the region being studied, which is then used to calculate co-seismic and post-seismic stress using PSCMP.

Depth (km)	**Vp (km/sec)**	**Density (kg/m^3)**		
0-32	6	2720	Upper Crust	Elastic
32-47	6.3	2790	Lower Crust	Viscoelastic
47-64	6.6	2850		
64-100	7.8	3250	Upper Mantle	

Table 4.1 Parameters of 1D multilayered model

Based on all these parameters we designed the Crustal Model for the region with various friction and viscosity values which is given below in Figure4.1.

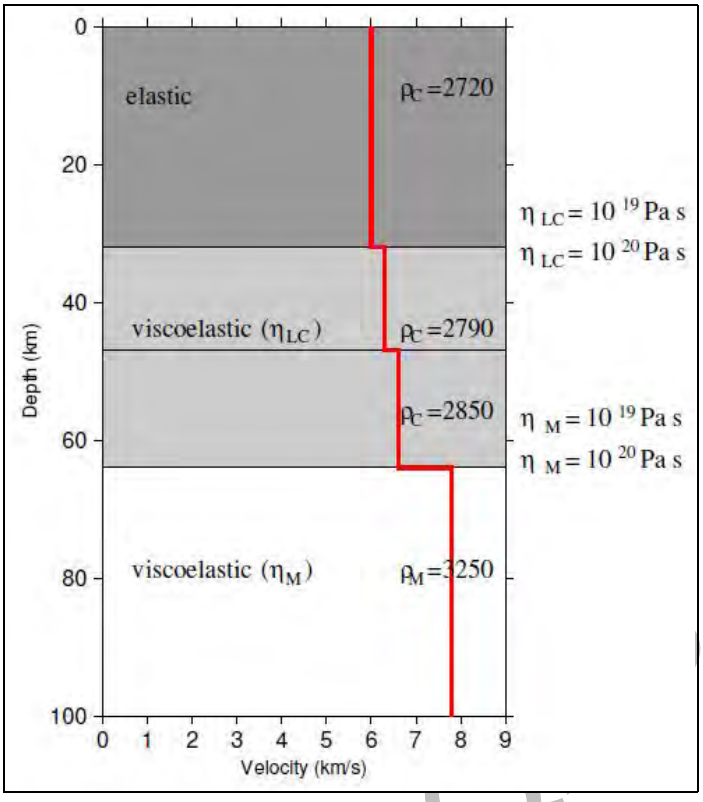

Figure 4.1 Crustal Model with varying viscosities in Lower Crust and Upper Mantle.

4.3 Computation of Green function

The Green's function is defined empirically as the impulse response of the medium. With regard to a signal being received by sensors at two different locations, the Green's function translates to Earth's response between two receivers. Based on the structure (1D velocity model) of our study area for which we want to calculate the stresses, and to analyze the response of the stresses that how it will behave, computation of green function is necessary.

For the computation of green function, we will have to set the input file that comprised of multiple parameters, which are used for the calculation of green function.

The input file for the FORTRAN77 software 'PSGRN' which is used to compute the responses (Green's function) of a multilayered viscoelastic half-space to point dislocation sources buried at various depths. For our studies, we chose the 10km as seismogenic depth. PSGRN software is also used for the calculation of time-dependent viscoelastic relaxation.

4.3.1 Parameters for Green function Input file

No	Parameters	Description
1	**Source-observation conFigureurations**	a. The first parameter for source-observation conFigureurations includes the depth and the type of earthquake. The point on which observation will be taken, what will be its depth because on a particular depth, Green function response will be generated. Normally, Green function is generated at 10km depth because it is a seismogenic depth but if we want to plot the cross-section, then the depth can be selected at 5km, 10km or 15km etc for the computation of green function depending on the objectives. Next, we must have to choose between oceanic (0) or continental (1) The earthquakes with same depth of the observation points (km). We selected 10km depth of the observation points and switched for continental (1) earthquakes for the computation of green function. b. Second step includes: • Number of observations. • Start and end distance and the interval between them. Less interval leads to increase in resolution due to which computational time also increases and vice versa. c. Third is the number of equidistant source depth.

2	**Time-sampling**	It includes: a. Number of time samples and time-window. For how many number of days, green function is calculated.
3	**1-D velocity model**	It includes depth, Vp, Vs, Rho, as well as lower crust and upper mantle viscosities.

Table 4.2 Parameters for Green function Input file

4.3.2 Output file

No	Parameters	Description
1.	**3 Displacement components file names**	Uz, ur and ut are the three displacement components that will be determined.
2.	**6 Stress components file names**	The 6 stress components which will be calculated i.e. szz, srr, stt, szr, srt,stz

Table 4.3 Parameters for green function output file

4.4 Computation of Stresses

After the calculation of green function using program 'PSGRN', 'PSCMP' program is employed for the co-seismic and post-seismic stresses calculation based on Green function, already computed employing the 'PSGRN' program. An arbitrary number of rectangular dislocation planes depicts the earthquake source.

After the calculation of green function, we have to compute the CFS caused by the respective earthquake on the earthquakeas well as on the nearby faults of the region.

4.4.1 Parameters for Stresses computation input file

No	Parameters	Description
1	**Observation array**	The first parameter includes which type of observation will be selected. Observation array can be selected by three ways: a. Irregular observation position, for this

		observation position we have to select (=0). b. 1D observation profile, in this profile starting and ending latitude longitude positions are given after which it plot the lines automatically. For this profile we have to select (=1) c. Rectangular 2D observation array, in this array , the latitude and longitude positions of every given point is required. For this we have to select (=2)
2	**Orientation of receiver faults**	Second parameter includes the orientation of the receiver fault: a. Selection of (1/0) for los displacements (only for snapshots). It will remain fixed. b. For coulomb stress changes, select (1/0) output (only for snapshots): The consistent regional master fault mechanism is described by icmb, friction (which varies from 0.2-0.8), Skempton Ratio, Strike, Dip and Rake angles. In arbitrary order, the uniform regional principle stresses i.e sigma1, sigma 2 and sigma 3 (Pa) triggering value-(0.0.1 Mpa). The orientation of the pre-stress field will be calculated considering that the master fault is suitably oriented according to the Coulomb failure stress criterion. The following information will be included in the snapshots if this option is set i.e icmb=1. On the master fault, CMB_Fix, Sig_Fix= Coulomb and normal stress changes. Str_Op1/2, Dip_Op1/2, Slp_Op1/2=strike, dip and rake angles of the two optimally oriented faults**.**

		c. Output directory in char format i.e outdir d. Output for components of displacement selection (1/0=(yes/no) e. Selection of file name for the x,y and z components. f. Outputs for stress components selection (1/0=yes/no) g. Choosing a file name for all the six components of stress i.e xx, yy, zz, xy, yz and zx respectively.
3	**Green's Function Database**	a. A directory containing green function. We have to give the path of the green function here. b. File names for the Green's function: 3 displacement components 4 stress components

Table 4.4 Parameters for Stress computation input file

CHAPTER 05

NUMERICAL MODELING OF CO-SEISMIC AND POST-SEISMIC STRESS CHANGES

We calculated the co-seismic and post-seismic stress changes caused by the earthquake sequence, which originated in 1905 and ended in 2005, using elastic deformation theory and a multi-layered lithospheric model. We also looked at the relationship between these events, as well as the impact of one earthquake on the upcoming ones.

For the computation of both co- and post-seismic stress, the lower crust and upper mantle are assumed to be fully elastic. Because of post-seismic viscoelastic relaxation, co-seismic stress changes in the lower crust and upper mantle can be transferred upwards to the seismogenic upper crust. The co-seismic as well as post-seismic effects caused by the 1905-2005 earthquake sequence are depicted in the Figures below. Our main findings are derived from using moderate viscosities (1×10^{19} and 1×10^{20} Pa.s) for both the lower crust and upper mantle to approximate seismic stress changes.

5.1 Co-seismic Stress changes

5.1.1 The 1905 Earthquakes

The 7.7Mw Kangra earthquake occurred on April, 04 1905 with the epicentral location (33.0°N, 76.15°E). This earthquake is strike-slip in nature, which was occurred on MCT fault. Inferred from scaling law (Table 3.1), computed results are reported in table 3.2, the rupture length is 98km, rupture width is 35.2km, and uniform slip is 0.8m of 1905 earthquake. Based on stress triggering theory and multilayered model of lithosphere, we calculated the coulomb stress changes of co-seismic event caused by 1905 Kangra earthquake, Stress map reported in Figure 5.1. From the focal mechanism solution of the Mw 7.7, 1905 event, the earthquake parameters are taken as strike=85°, dip= 5° and rake angle=110°.

Figure5.1 reports the co-seismic coulomb stress changes at a depth of ~20km with various effective co-efficient of friction such as 0.2, 04 and 0.6 caused by this earthquake. Different co-efficient of frictions are showing different pattern and rate of stress transfer in the surrounding. The significant features are the presence of lobes created by the stress release/transfer by the 1905 earthquake. The warm red, indicating the regions with increasing/Positive Coulomb stress due to co-seismic slip on the faults which is transferring the coulomb stress in surrounding areas and can triggers the seismic activity. The blue lobes indicating the stress shadow zones with decreased coulomb stress, the region which has released the stress on faults, and eventually may depress the forthcoming seismic activity.

Figure5.1 shows that the stress transfer of co-seismic static caused by the 1905 Kangra earthquake leads the CFS increase on the North-west and south-eastern part which is shown by red lobes, and CFS decrease on the North-east and south-western part which can be seen in blue lobes. As we can see in Figure this event is highly affected the area in terms of stresses, because it was high magnitude earthquake of 7.7Mw. So this earthquake is one of the devastating disaster in the history which affected the sub-Himalayan Hills.

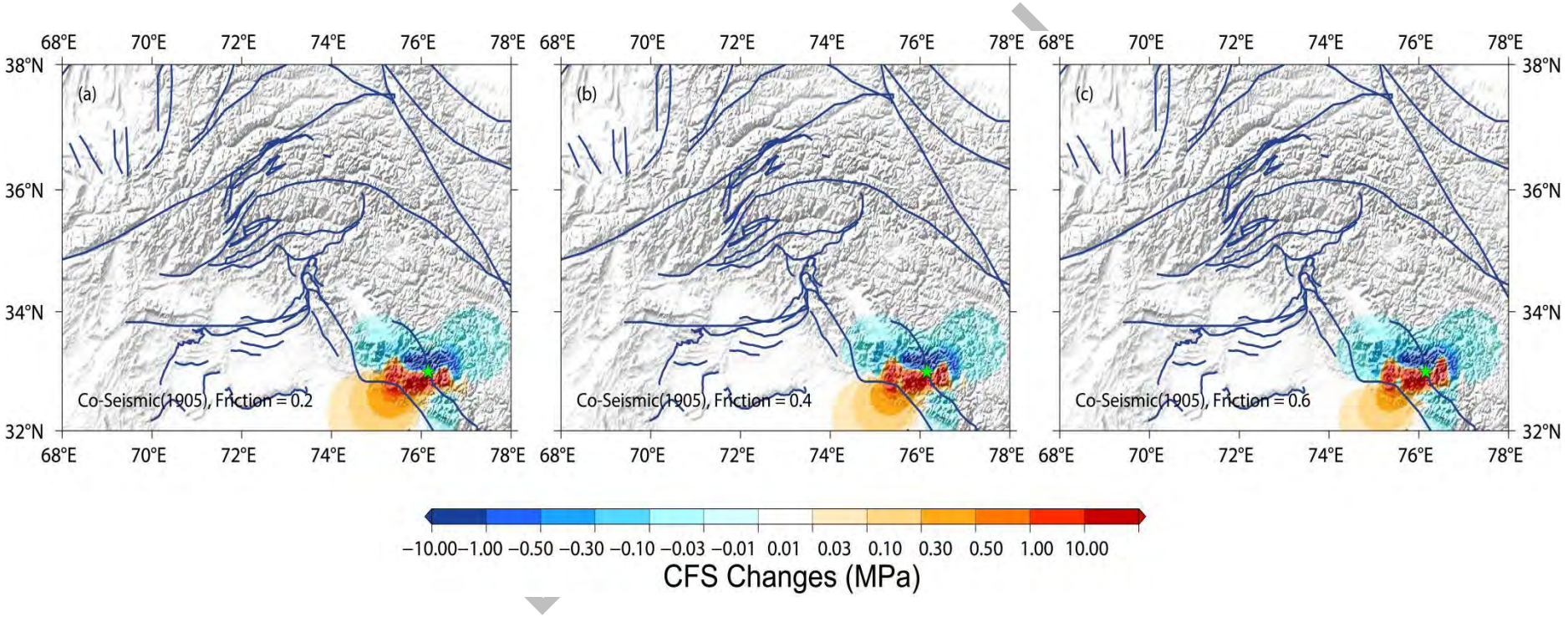

Figure 5.1 Stress Maps of Co-seismic CFS of 1905 Earthquake with various co-efficient of friction (0.2, 0.4, and 0.6 represented as a, b, c respectively).

5.1.2 The 1972 Earthquake

The earthquake of 1972 with the magnitude of 6.2Mw occurred on 3rd September, with the epicenter located at (35.12°N, 73.42°E). Inferred from scaling law (Table 3.1), computed results are reported in table 3.2, the rupture length is 11.1km, rupture width is 8.6km, and uniform slip of earthquake is 0.6m respectively.

Figure5.2 reports the co-seismic coulomb stress changes at a depth of ~30km with various co-efficient of friction of 0.2, 0.4 and 0.6. From the focal mechanism solution of the 1972 earthquake, the earthquake parameters are taken as strike=270°, dip= 29° and rake angle=125. This earthquake is thrust in nature with strike-slip component, which was occurred on MKT fault. Co-seismic coulomb stress changes associated with 1972 earthquake shows that this event has generated positive stress on the Eastern and Western part which indicating stressed regions and negative stress on Northern and Southern lobe. The surroundings of epicentral is showing low stress transfer and failure because of magnitude of 6.2Mw.

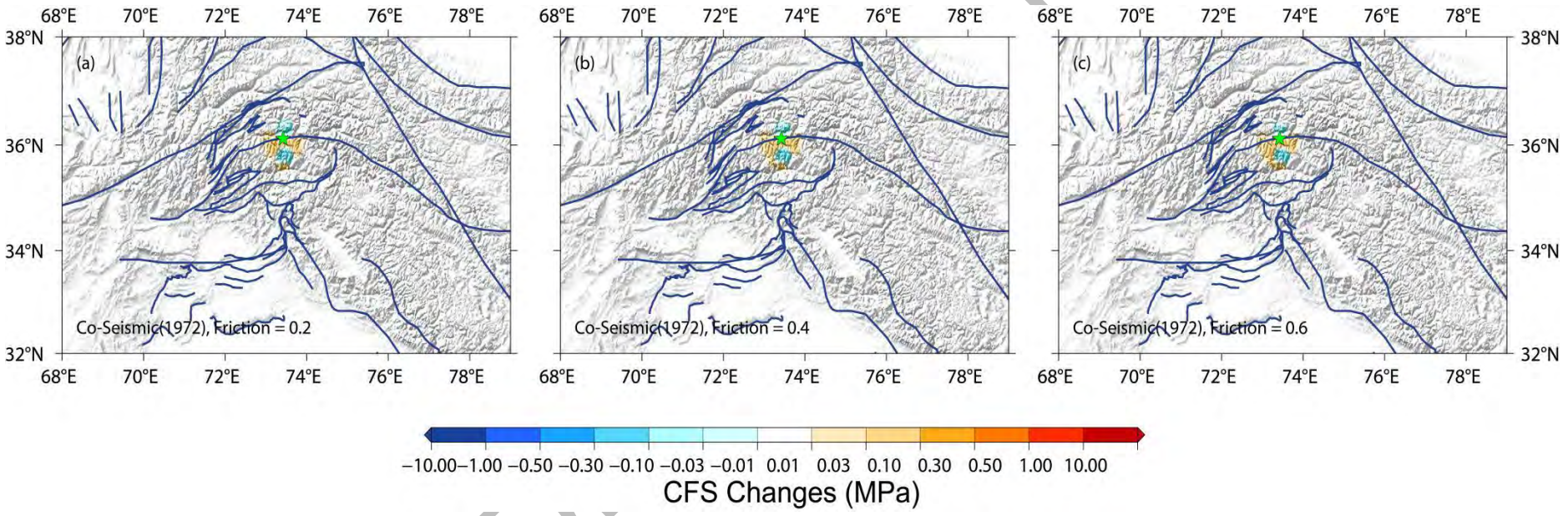

Figure 5.2 Stress Maps of Co-seismic CFS of 1972 Earthquake with various co-efficient of friction (0.2, 0.4, and 0.6 represented as a, b, c respectively).

5.1.3 The 1981 Earthquake

The 6.1Mw, 1981 earthquake occurred on September 12th, with the epicentre at (35.32°N, 73.48°E). The rupture length of the earthquake is 9.6km, the rupture width is 9km, and the uniform slip of the earthquake is 0.6m, as derived from the (Table 3.1), and the computed results are listed in table 3.2.

Figure5.3 illustrates the changes in co-seismic coulomb stress at a depth of 10km with three effective co-efficient of friction such as 0.2, 0.4, and 0.6. The earthquake parameters are taken from the focal mechanism solution of the 1981 earthquake as strike=107°, dip=36°, and rake angle=79. This is a thrust earthquake in nature with strike-slip component, which was occurred on MMT fault. The co-seismic coulomb stress changes are associated with the 1981 earthquake show that this event generated positive stress on the east and west sides closer to the epicentre, while the northern, southern, and a few parts of the lobe in west indicating negative stress.

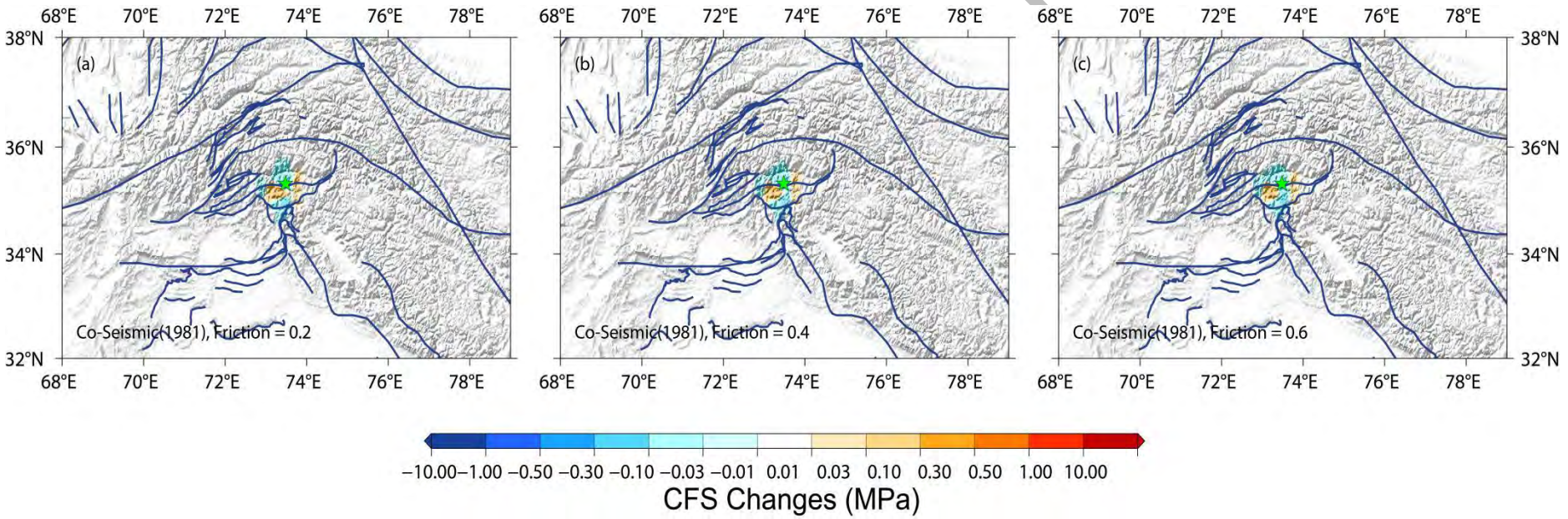

Figure 5.3 Stress Maps of Co-seismic CFS of 1981 Earthquake with various co-efficient of friction (0.2, 0.4, and 0.6 represented as a, b, c respectively).

5.1.4 The 1982 Earthquake

The earthquake of 1982 with magnitude of 6.4Mw occurred on September 12th, with the epicentre at (36.40°N, 68.75°E). The rupture length of the earthquake is 14.9km, the rupture width is 12km, and the uniform slip of the earthquake is 0.6m, as derived from the (Table 3.1), and the computed results are listed in table 3.2.

Figure 5.4 illustrates the changes in co-seismic coulomb stress at a depth of 12km with three effective co-efficient of friction such as 0.2, 0.4, and 0.6. The earthquake parameters are taken from the focal mechanism solution of the 6.4Mw, 1982 Earthquake as strike=218°, dip=43°, and rake angle=114. The earthquake is thrust in nature with strike slip component, which was occurred on Herat fault. The co-seismic coulomb stress changes are associated with the 1982 earthquake show that this event generated positive stress on the North-western and South-eastern region while the lobes in North-eastern and South-western indicating negative stress.

According to the magnitude of this earthquake and the CFS lobes, this event seems to have accountable stress transfer on its surroundings. The direction of stress release and failure is changing with respect to change in friction, which can be clearly seen in the Figure 5.4(a, b, and c). The stress transfer becomes softly far from the epicenter as friction is increasing.

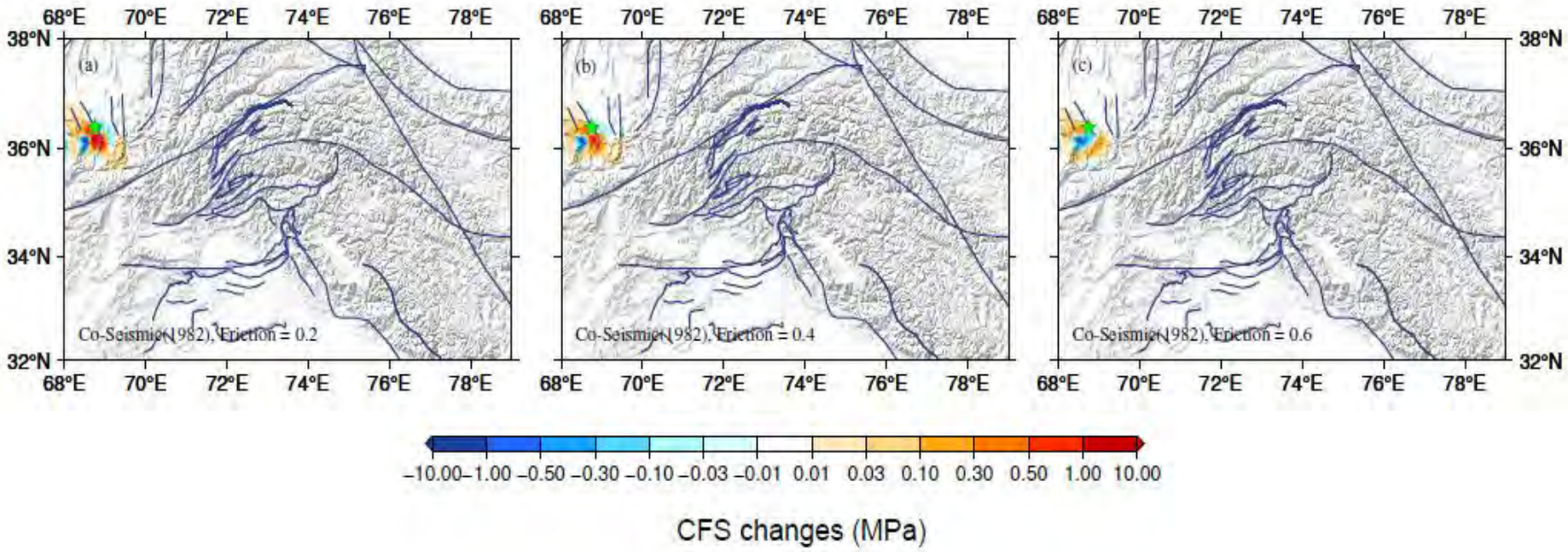

Figure 5.4 Stress Maps of Co-seismic CFS of 1982 Earthquake with various co-efficient of friction (0.2, 0.4, and 0.6 represented as a, b, c respectively).

5.1.5 The 1984 Earthquake

The earthquake of 1984, with magnitude of 6.1Mw occurred on 1st February, with the epicentre at (34.59°N, 70.5°E). The rupture length of the earthquake is 9.6km, the rupture width is 9km, and the uniform slip of the earthquake is 0.6m, as derived from the (Table 3.1), and the computed results are listed in table 3.2.

Figure5.5 illustrates the changes in co-seismic coulomb stress at a depth of 25km with three effective co-efficient of friction such as 0.2, 0.4, and 0.6. The earthquake parameters are taken from the focal mechanism solution of the 1984 earthquake as strike=268°, dip=37°, and rake angle=121. The earthquake is thrust in nature with strike slip component, which was occurred on MKT fault. The co-seismic coulomb stress changes are associated with the 1984 earthquake show that this event generated positive stress on the North-western side, but due to various friction rate the direction of positive stress is also changing in Southward. The blue lobes which is equally closer from all direction to the epicenter are indicating negative stress. According to the magnitude of the earthquake and the CFS lobes, this event is showing very low stress transfer and failure on its surroundings.

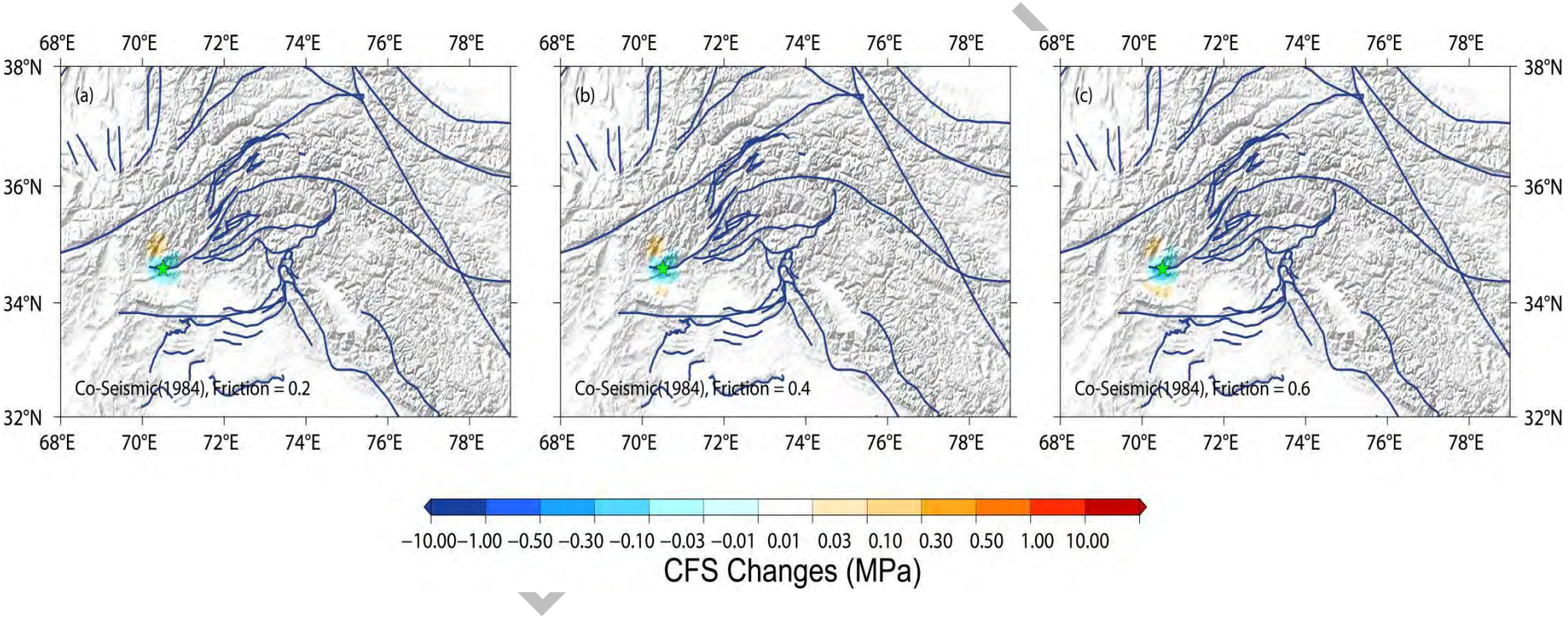

Figure 5.5 Stress Maps of Co-seismic CFS of 1984 Earthquake with various co-efficient of friction (0.2, 0.4, and 0.6 represented as a, b, c respectively).

5.1.6 The 1990 Earthquake

The earthquake of 1990 with the magnitude of 6.1Mw, occurred on 5th of March 10, with the epicentre at (36.40°N, 73.0°E). The rupture length of the earthquake is 9.6km, the rupture width is 9km, and the uniform slip of the earthquake is 0.6m, as derived from the (Table 3.1), and the computed results are listed in table 3.2.

Figure5.6 illustrates the changes in co-seismic coulomb stress at a depth of 20km with three effective co-efficients of friction such as 0.2, 0.4, and 0.6. The earthquake parameters are taken from the focal mechanism solution of the 1990 earthquake as strike=192°, dip=36°, and rake angle=-46. This earthquake is normal in nature with strike slip component, which was occurred on Herat fault. The co-seismic coulomb stress changes are associated with the 1990 earthquake shows that the event transferred positive stress on the South-western part mainly, but as well as few release of stress(red lobes) can been seen in in north and east part. while the North-eastern part is indicating negative stress in terms of blue lobes.

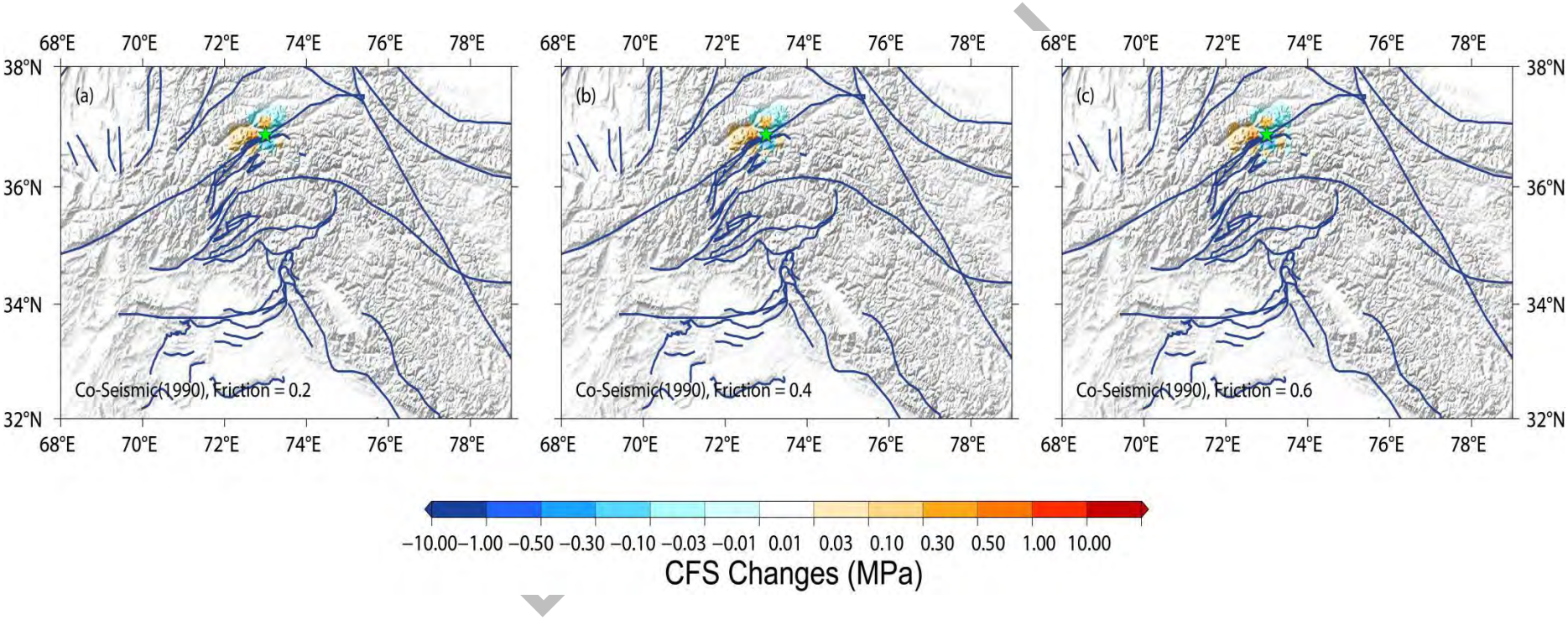

Figure 5.6 Stress Maps of Co-seismic CFS of 1990 Earthquake with various co-efficient of friction (0.2, 0.4, and 0.6 represented as a, b, c respectively).

5.1.7 The 1992 Earthquake

The earthquake of 1992, with magnitude of 6.0Mw occurred on 20th of May, with the epicentre at (32.95°N, 71.27°E). The rupture length of the earthquake is 8.3km, the rupture width is 7.1km, and the uniform slip of the earthquake is 0.5m, as derived from the (Table 3.1), and the computed results are listed in table 3.2.

Figure5.7 illustrates the changes in co-seismic coulomb stress at a depth of 15km with three effective co-efficient of friction such as 0.2, 0.4, and 0.6. The earthquake parameters are taken from the focal mechanism solution of the 1992 earthquake as strike=237°, dip=5°, and rake angle=79. The earthquake is strike-slip in nature, which was occurred on Sarghar fault. The co-seismic coulomb stress changes are associated with the 1992 earthquake show that the event transferred positive stress on the North-eastern and South-western side (red lobes), while the North-western and South-western part is indicating negative stress in blue lobes.

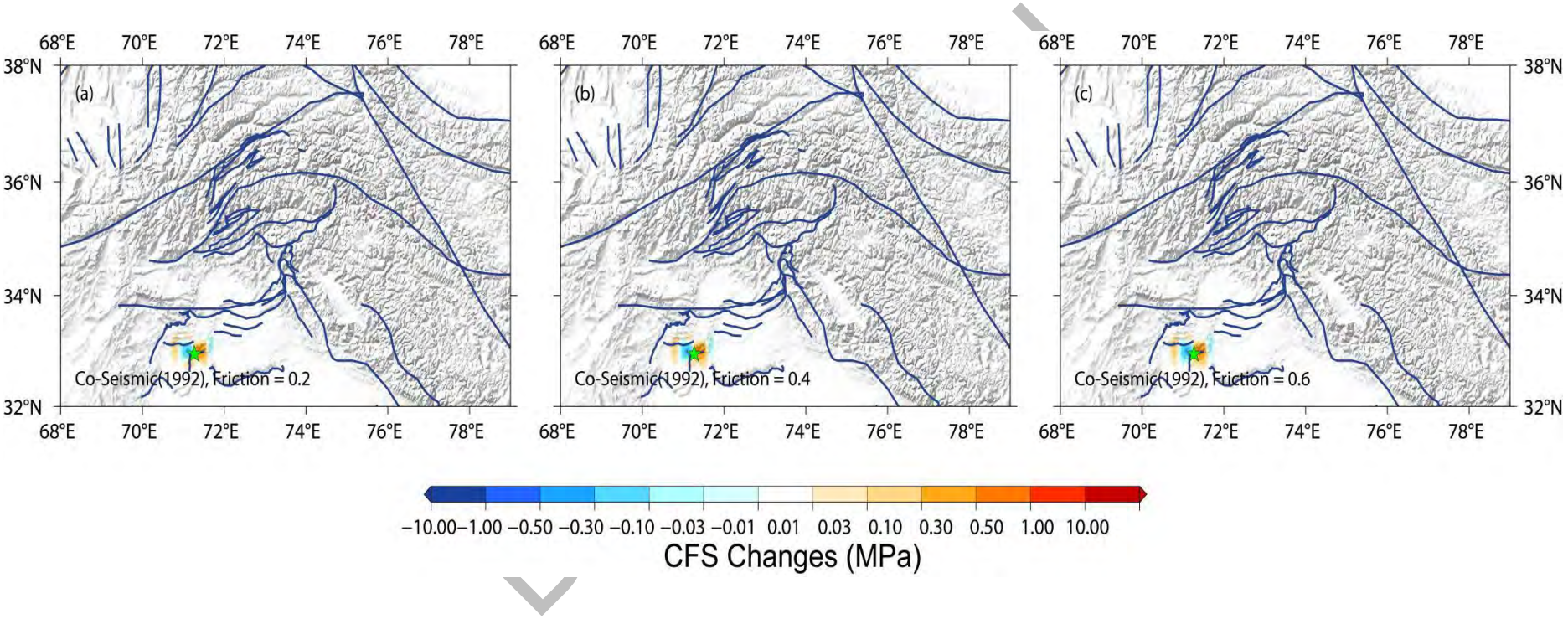

Figure 5.7 Stress Maps of Co-seismic CFS of 1992 Earthquake with various co-efficient of friction (0.2, 0.4, and 0.6 represented as a, b, c respectively).

5.1.8 The 1996 Earthquake

The earthquake of 1984, with magnitude of 6.8Mw occurred on 19th of November, with the epicentre at (35.45°N, 77.86°E). The rupture length of the earthquake is 24.5km, the rupture width is 17.4km, and the uniform slip of the earthquake is 0.7m, as derived from the (Table 3.1), and the computed results are listed in table 3.2.

Figure5.8 illustrates the changes in co-seismic coulomb stress at a depth of 15km with three effective co-efficient of friction such as 0.2, 0.4, and 0.6. The earthquake parameters are taken from the focal mechanism solution of the 1996 earthquake as strike=180°, dip=71°, and rake angle=170. The earthquake is normal in nature with strike-slip component, which was occurred on Karakoram fault. The co-seismic coulomb stress changes are associated with the 1996 earthquake show that this event transferred positive stress on the East to South-eastern part in red lobes, while the North-eastern and South-western part is indicating negative stress in blue lobes. According to the magnitude of the 6.8Mw and the CFS lobes, this event is showing accountable stress transfer and failure on its surroundings.

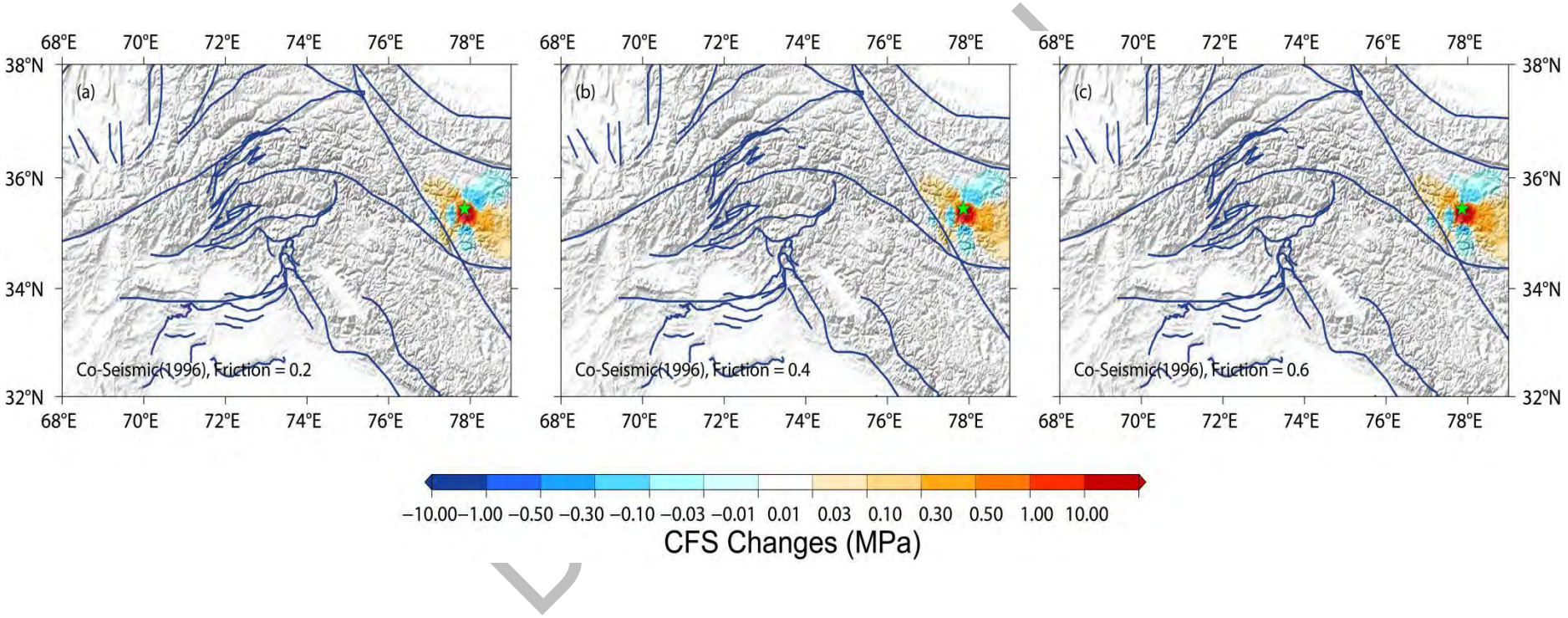

Figure 5.8 Stress Maps of Co-seismic CFS of 1996 Earthquake with various co-efficient of friction (0.2, 0.4, and 0.6 represented as a, b, c respectively).

5.1.9 The 1998 Earthquake

The earthquake of 1998, with magnitude of 6.6Mw occurred on 30th of May, with the epicentre at (37.7°N, 70.45°E). The rupture length of the earthquake is 19.5km, the rupture width is 14.8km, and the uniform slip of the earthquake is 0.5m, as derived from the (Table 3.1), and the computed results are listed in table 3.2.

Figure5.9 illustrates the changes in co-seismic coulomb stress at a depth of 30km with three effective co-efficient of friction such as 0.2, 0.4, and 0.6. The earthquake parameters are taken from the focal mechanism solution of the 1998 earthquake as strike=111°, dip=85°, and rake angle=175. The earthquake is normal dip slip in nature, which was occurred on Herat fault. The co-seismic coulomb stress changes are associated with the 1998 earthquake show that this event transferred positive stress on the Western and Southern sides, while the Northern and Eastern sides are indicating negative stress in blue lobes.

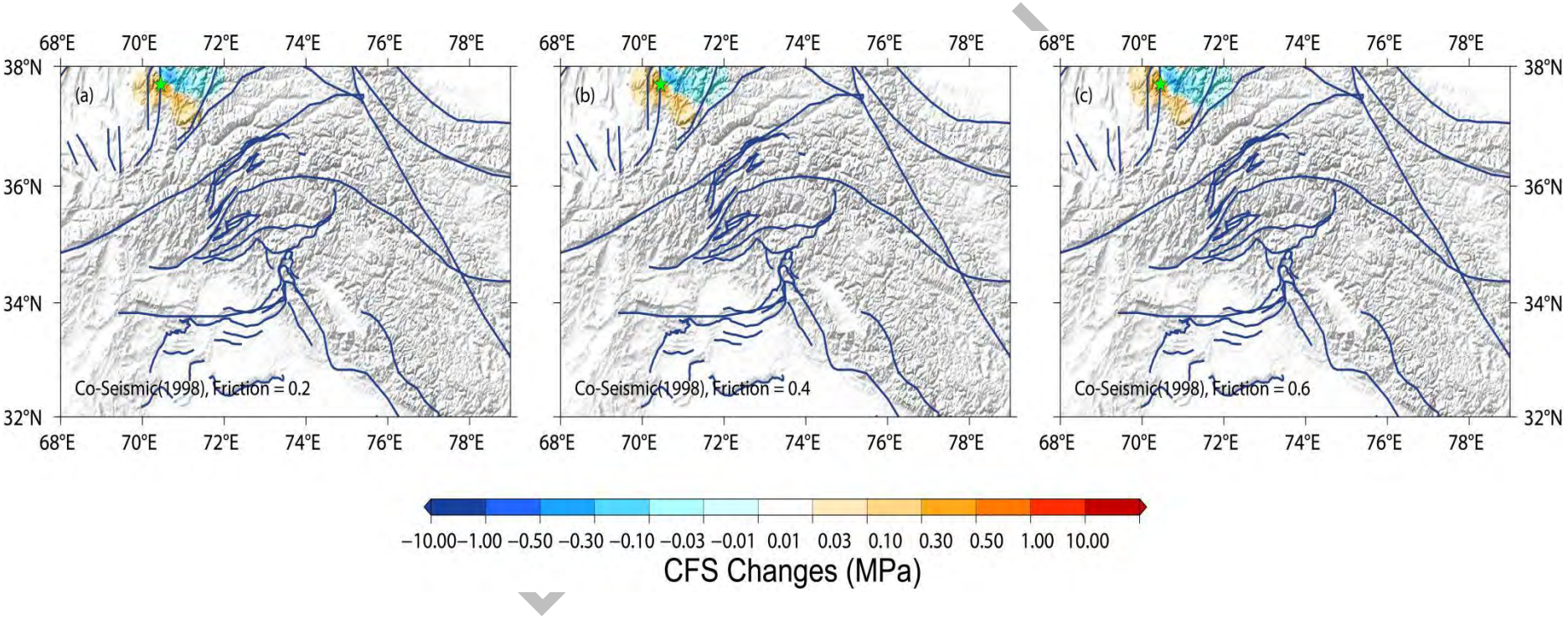

Figure 5.9 Stress Maps of Co-seismic CFS of 1998 Earthquake with various co-efficient of friction (0.2, 0.4, and 0.6 represented as a, b, c respectively)

5.1.10 The 2002 Earthquake

The earthquake of 2002, with magnitude of 6.3Mw occurred on 20th of November, with the epicentre at (35.40°N, 74.64°E). The rupture length of the earthquake is 12.9km, the rupture width is 9.4km, and the uniform slip of the earthquake is 0.6m, as derived from the (Table 3.1), and the computed results are listed in table 3.2.

Figure5.10 illustrates the changes in co-seismic coulomb stress at a depth of 15km with three effective co-efficient of friction such as 0.2, 0.4, and 0.6. The earthquake parameters are taken from the focal mechanism solution of the 2002 Earthquake as strike= 209°, dip= 42°, and rake angle= -170. The earthquake is normal in nature, which was occurred on Raikot fault. The co-seismic coulomb stress changes are associated with the 2002 earthquake shows that the event transferred positive stress on the Northern side as well as less stress release can be seen on South-eastern side, while the negative stress can be seen closer to the epicenter which is distributing in all direction.

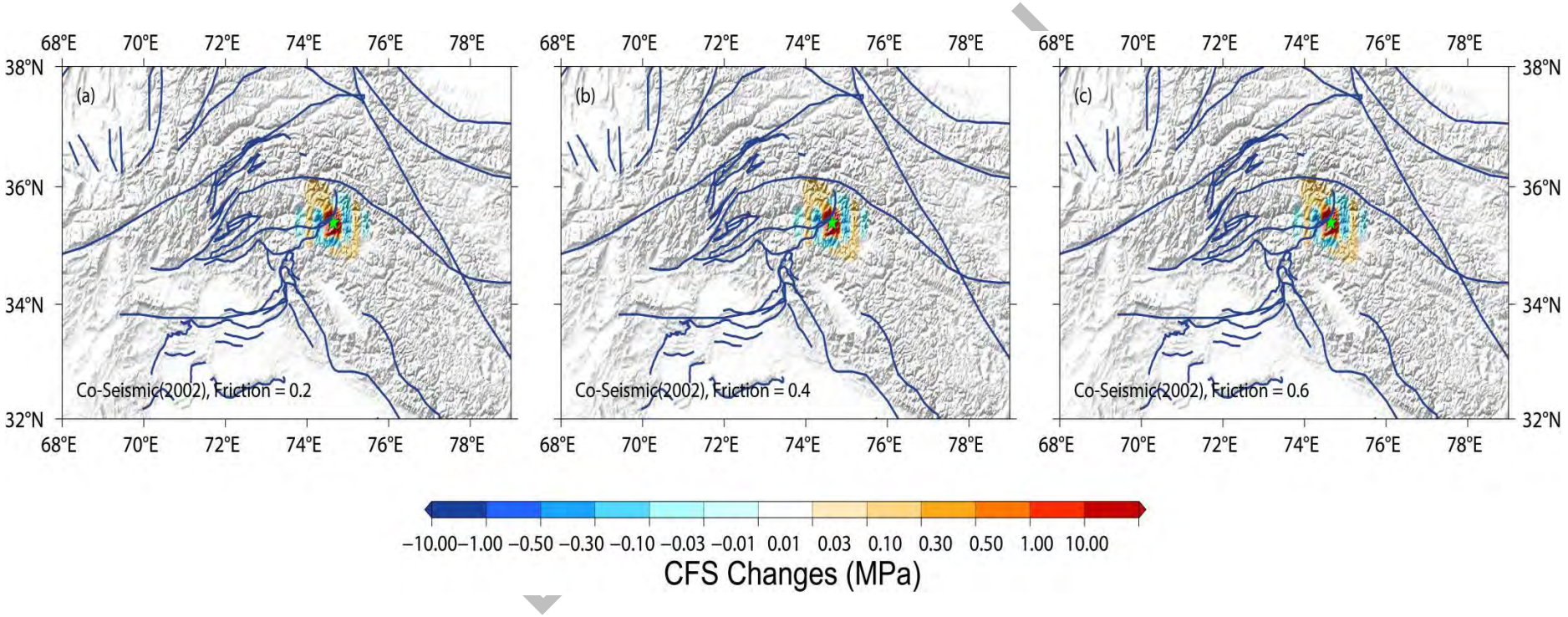

Figure 5.10 Stress Maps of Co-seismic CFS of 2002 Earthquake with various co-efficient of friction (0.2, 0.4, and 0.6 represented as a, b, c respectively).

5.1.11 The 2005 Kashmir Earthquake (Main Shock)

The Kashmir earthquake, with the magnitude of 7.5Mw occurred on 8th of October, with the epicentre at (34.43°N, 73.64°E). For this earthquake the complete Rupture model with all parameters such as rupture length, width and slip is given in the Appendices.

Figure5.11 illustrates the changes in co-seismic coulomb stress at a depth of 8km with an effective co-efficient of friction 0.4. The earthquake parameters are taken from the focal mechanism solution of the 2005 earthquake as strike=331°, dip=29°, and rake angle=125. The earthquake is thrust in nature with strike-slip component, which was occurred on MBT fault. The co-seismic coulomb stress changes are associated with the 2005 earthquake show that the event is transferring the positive stress from North to North-eastern, South to South-western, and in western part as well. While the Eastern, Western, South-eastern, and North-western side, is indicating negative stress. This earthquake is showing huge amount of stress transfer in its surroundings. Rate of stress transfer is very high closer to the epicenter which is clearly visible in red shadow zone. According to the magnitude of the 6.4 Mw and the CFS lobes, this event is showing accountable stress transfer and failure on its surroundings.

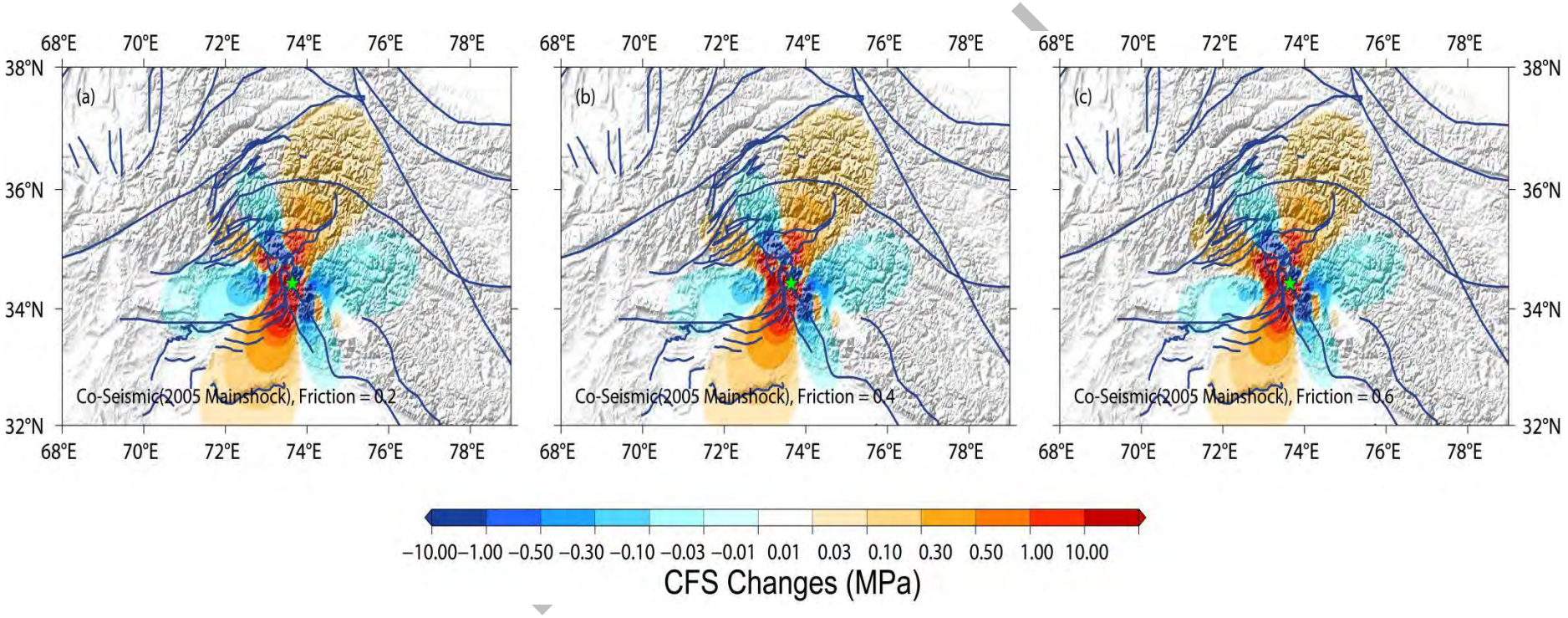

Figure 5.11 Stress Maps of Co-seismic CFS of 2005 Earthquake (Main shock) with various co-efficient of friction (0.2, 0.4, and 0.6 represented as a, b, c respectively).

5.1.12 The 2005 Kashmir Earthquake (After Shock)

The Kashmir earthquake, with magnitude of 6.4Mw occurred on 8th of October, with the epicentre at (34.94°N, 73.10°E). The rupture length of the earthquake is 14.9km, the rupture width is 10.3km, and the uniform slip of the earthquake is 0.6m, as derived from the (Table 3.1), and the computed results are listed in table 3.2.

Figure5.12 illustrates the changes in co-seismic coulomb stress at a depth of 15km with three effective co-efficient of friction such as 0.2, 0.4, and 0.6. The earthquake parameters are taken from the focal mechanism solution of the 2005 earthquake as strike=328°, dip=39°, and rake angle=107. The earthquake is thrust in nature with strike slip component, which was occurred on MBT fault. The co-seismic coulomb stress changes are associated with the 2005 earthquake show that the event transferred positive stress on the Northern and Southern side, while the Eastern and North-western part is indicating negative stress in blue lobes. With respect to change in friction the stress distribution is also varying in direction.

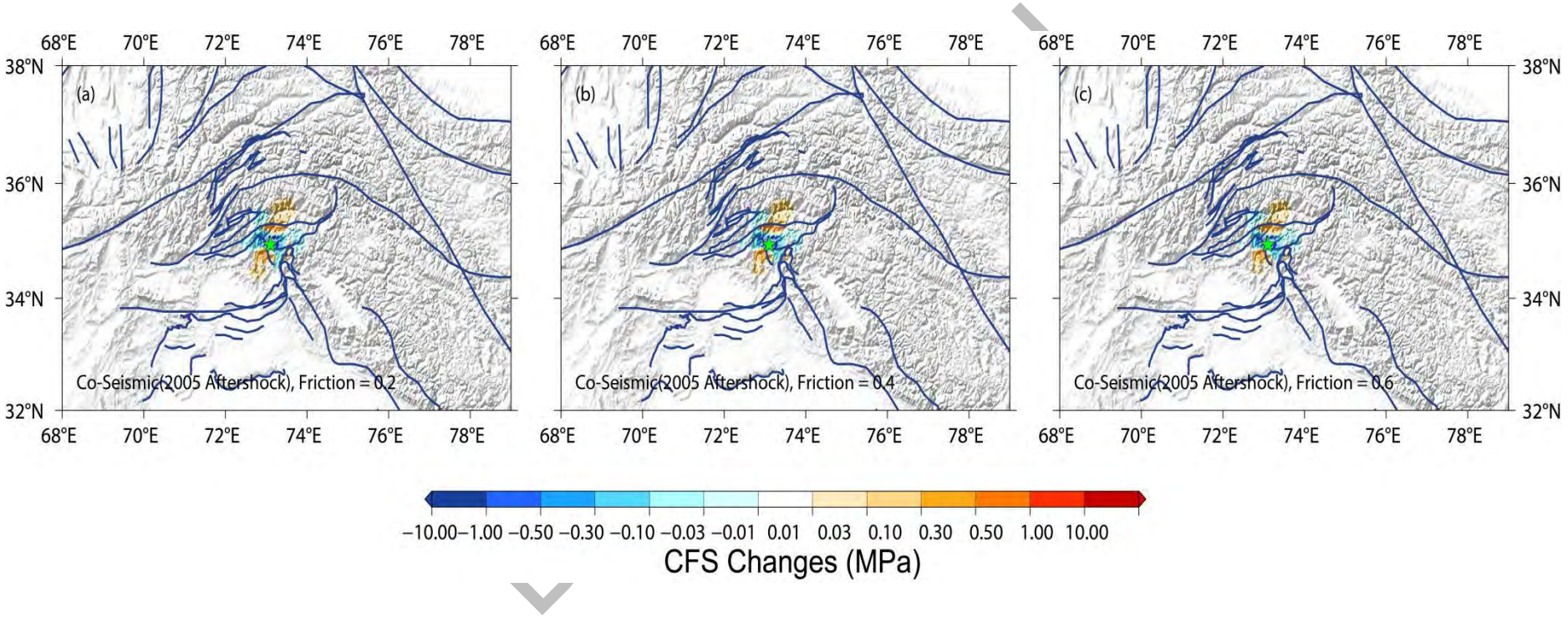

Figure 5.12 Stress Maps of Co-seismic CFS of 2005 Earthquake (Aftershock) with various co-efficient of friction (0.2, 0.4, and 0.6 represented as a, b, c respectively).

5.2 Robustness of Numerical Results

To verify the robustness of our results, we conducted numerous simulations with different combinations of following two factors:

a. Co-efficient of friction.
b. Effect of viscosity.

Table 5.1 shows the parameterized values of co-efficient of friction, lower crust, and upper mantle viscosities used in simulations to test the robustness of our results.

5.2.1 Co-efficient of friction (μ')

The selection of the most appropriate value for the effective co-efficient of friction is of minor importance for the model because it regulates only the normal stress contribution to the CFS (King et al., 1994). The coefficient varies depending on the type of fault, with higher values (0.6-0.8) for thrust and normal faults and lower values (0.2-0.4) for strike-slip faults (Xiong et al., 2017). In the numerical computations, as previously stated, a reasonable value of 0.4 is used. Numerical studies show that the computed stress varies with the co-efficient of friction, the viscosity of the lower crust, and the viscosity of the upper mantle. The results are compiled in (Figures 5.1 to 5.19).

5.2.2 Viscosity

Even though viscoelastic relaxation has been used in the calculations, the viscosities of the lower crust and upper mantle are critical in computing the time-dependent stress-field. In this study, we used viscosities that are consistent with the results of previous studies on post-seismic deformation. (Ryder et al. 2007) and (Shao et al. 2016) Because of a lack of continuous observation of post-seismic deformation in the examined region, the viscosities of the crust and upper mantle are not adequately constrained. As a result, we experimented with various viscosity values to ensure the results' durability.

Table 5.1 shows the results of two different simulations with varying values of effective co-efficient of friction and lower crust and upper mantle viscosities. Further the Crustal Model of varying viscosities in upper mantle and lower crust is given in

Figures 5.13 to 5.18. The results of simulation I are shown in Figures 5.13, 5.14, and 5.15, those of simulation II in Figures 5.16, 5.17, and 5.18 respectively.

Simulations	Viscosity	Friction
I.	Lower Crust = $\mathbf{1\times10^{19}}$ Pa s	μ′= 0.2
	Upper Mantle = $\mathbf{1\times10^{19}}$ Pa s	μ′= 0.4
		μ′= 0.6
II.	Lower Crust = $\mathbf{1\times10^{20}}$ Pa s	μ′= 0.2
	Upper Mantle = $\mathbf{1\times10^{20}}$ Pa s	μ′= 0.4
		μ′= 0.6

Table 5.1 Simulations of result with various values of viscosity and friction

Based on all these parameters we designed the Crustal Model for the region with various friction and viscosity values which is given below:

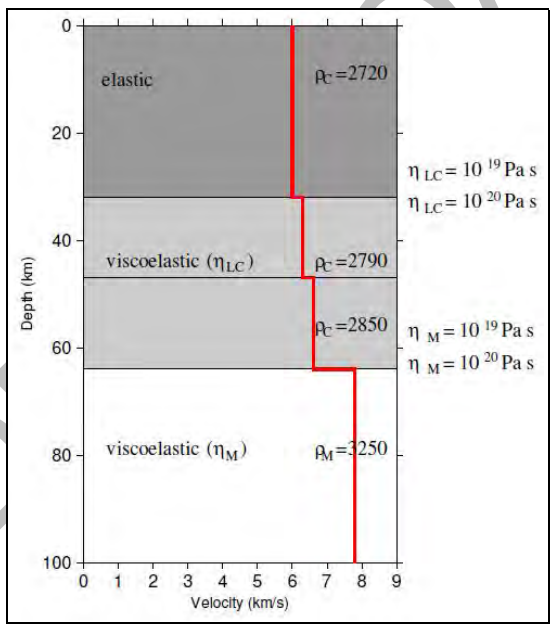

Figure 5.13 Crustal Model with varying viscosities in Lower Crust and Upper Mantle.

The simulation results demonstrate that choosing a lower viscosity resulted in a rapid relaxation, which eventually resulted in a rapid stress accumulation, and likewise. This is because a lower viscosity value speeds up the post-seismic viscoelastic relaxation process. The viscoelastic flow is caused by the co-seismic stress changes that take place after the co-seismic elastic deformation (Freed et al., 2005). The lower crust's viscosity primarily governs the rate of stress transfer; the lower the viscosity, the faster the transfer speed, and vice versa. Our tests with

different viscosity values revealed that, while the magnitude of CFS varies slightly, it has no effect on the CFS pattern as well as the triggering relationship as among sequences over the time span of this study (Verdecchia & Carena, 2015).

5.3 Post- Seismic Stress changes Results

From the above-mentioned combination of various friction (0.2, 0.4, and 0.6), and two different model of simulation with varying viscosities of the lower Crust and the upper Mantle the following results are computed:

5.3.1 The 1905 Earthquake

The maximum and minimum ΔCFS changes caused by 1905 Kangra earthquake event are 2.636MPa and -1.736MPa respectively. The Stress map of post-seismic stresses caused by the 1905 earthquake's viscoelastic relaxation is given in Figures 5.14, 5.15, 5.16, 5.17, 5.18, and 5.19(a). The significant contribution of viscoelastic stress transfer is manifested in the Stress map, where the size of the lobes has increased.

5.3.2 The 1972 Earthquake

There is 67 years of gap between 1905 Kangra earthquake and 1972 earthquake, Maxwell body model has been used to simulate post-seismic viscoelastic relaxation and quantify the impact of 1905 kangra earthquake on the 1972 earthquake in Figure5.2. The stress field state is then presented for a period just before each subsequent event. The ΔCFS immediately before the 1972 earthquake is shown in Figure 5.2, which is indicating the position of the stresses associated with the 1905 earthquake with the occurrence of the subsequent event. Figure5.2 indicates that 1972 earthquake is an independent earthquake. There is no interaction between these two events which indicates that it has not been triggered by the preceding earthquake, which is given in Figures 5.14, 5.15, 5.16, 5.17, 5.18, and 5.19(b). The maximum and minimum ΔCFS changes caused by 1972 earthquake event are 0.09609MPa and -0.1726MPa respectively.

5.3.3 The 1981 Earthquake

We have calculated the sequence for time-dependent stresses on active faults in the area after the earthquake of 1972, since the post seismic stress after the earthquake will influence the accumulation of stress on these faults as a function of time. According to the numerical results, the 1981 earthquake released the accumulated Coulomb stress on its surroundings, on which seismic activity has been depressed Figure5.3. As a result, the 1972 earthquake co-seismic static and post-seismic CFS changes are not interacting with the occurrence of the 1981 earthquake, which shows that 1981 earthquake has not been triggered by any of the previous earthquakes, hence we consider this earthquake as an independent event given in Figures 5.14, 5.15, 5.16, 5.17, 5.18, and 5.19(c). The maximum and minimum ΔCFS changes caused by 1981 earthquake event are 0.4147MPa and -0.265MPa respectively.

5.3.4 The 1982 Earthquake

We have calculated the sequence for time-dependent stresses on active faults in the area after the earthquake of 1981, since the post seismic stress after the earthquake will influence the accumulation of stress on these faults as a function of time. According to the numerical results, the 1982 earthquake released the accumulated Coulomb stress on its surroundings, in Figures 5.14, 5.15, 5.16, 5.17, 5.18, and 5.19(d). As a result, the 1981 earthquake co-seismic static and post-seismic CFS changes are not interacting with the occurrence of the 1982 earthquake, which shows that 1982 earthquake has not been triggered by any of the previous earthquakes, hence we consider this earthquake as an independent event. The maximum and minimum ΔCFS changes caused by 1982 earthquake event are 0.289MPa and -0.6536MPa respectively.

5.3.5 The 1984 Earthquake

We have calculated the time-dependent sequence of stress on active faults in the area after the 1982 earthquake since the post seismic stress after the earthquake will influence the accumulation of stress on these faults as a function of time. According to the numerical results, the 1984 earthquake released the accumulated Coulomb stress on its surroundings 5.14, 5.15, 5.16, 5.17, 5.18, and 5.19(e). As a result, the

1982 earthquake co-seismic static and post-seismic CFS changes are not interacting with the occurrence of the 1984 earthquake which shows that 1984 earthquake has not been triggered by any of the previous earthquakes, hence we consider this earthquake as an independent event. The maximum and minimum ΔCFS changes caused by 1984 earthquake event are 0.01532MPa and -0.273MPa respectively.

5.3.6 The 1990 Earthquake

We have calculated the sequence for time dependent stress on active faults in the area after the 1984 earthquake, since the post seismic stress after the earthquake will influence the accumulation of stress on these faults as a function of time. According to the numerical results, the 1990 earthquake released the accumulated Coulomb stress on its surroundings given in Figures 5.14, 5.15, 5.16, 5.17, 5.18, and 5.19(f) As a result, the 1984 earthquake co-seismic static and post-seismic CFS changes are not interacting with the occurrence of the 1990 earthquake which shows that 1990 earthquake has not been triggered by any of the previous earthquakes, hence we consider this earthquake as an independent event. The maximum and minimum ΔCFS changes caused by 1990 earthquake event are 0.4522MPa and -1.548MPa respectively.

5.3.7 The 1992 Earthquake

We have calculated time dependent sequence of the stress on active faults in the study area after the 1990 earthquake since the post seismic stress after the earthquake will influence the accumulation of stress on these faults as a function of time. According to the numerical results, the 1992 earthquake released the accumulated Coulomb stress on its surroundings in Figures 5.14, 5.15, 5.16, 5.17, 5.18, and 5.19(g). As a result, the 1990 earthquake co-seismic static and post-seismic CFS changes are not interacting with the occurrence of the 1992 earthquake which shows that 1992 earthquake has not been triggered by any of the previous earthquakes, hence we consider this earthquake as an independent event. The maximum and minimum ΔCFS changes caused by 1992 earthquake event are 0.4398MPa and -0.4751MPa respectively.

5.3.8 The 1996 Earthquake

We have calculated the time dependent sequence of stress on active faults in the area after the 1992 earthquake since the post seismic stress after the earthquake will influence the accumulation of stress on these faults as a function of time. According to the numerical results, the 1996 earthquake released the accumulated Coulomb stress on its surrounding given in Figures 5.14, 5.15, 5.16, 5.17, 5.18, and 5.19(h). As a result, the 1992 earthquake co-seismic static and post-seismic CFS changes are not interacting with the occurrence of the 1996 earthquake which shows that 1996 earthquake has not been triggered by any of the previous earthquakes, hence we consider this earthquake as an independent event. The maximum and minimum ΔCFS changes caused by 1996 earthquake event are 4.989MPa and -0.2174MPa respectively.

5.3.9 The 1998 Earthquake

We have calculated the sequence for time-dependent stress on active faults in the area after the 1996 earthquake, since the post seismic stress after the earthquake will influence the accumulation of stress on these faults as a function of time. According to the numerical results, the 1998 earthquake released the accumulated Coulomb stress on its surrounding given in 5.14, 5.15, 5.16, 5.17, 5.18, and 5.19(i). As a result, the 1996 earthquake co-seismic static and post-seismic CFS changes are not interacting with the occurrence of the 1998 earthquake which shows that 1998 earthquake has not been triggered by any of the previous earthquakes, hence we consider this earthquake as an independent event. The maximum and minimum ΔCFS changes caused by 1998 earthquake event are 0.3687MPa and 0.4178MPa respectively.

5.3.10 The 2002 Earthquake

We have calculated the sequence for time-dependent stress on active faults in the area after the 1998 earthquake since the post seismic stress after the earthquake will influence the accumulation of stress on these faults as a function of time. According to the numerical results, the 2002 earthquake released the accumulated Coulomb stress on its surrounding given in 5.14, 5.15, 5.16, 5.17, 5.18, and 5.19(j). As a result, the 1998 earthquake co-seismic static and post-seismic CFS changes are not

interacting with the occurrence of the 2002 earthquake which shows that 2002 earthquake has not been triggered by any of the previous earthquakes, hence we consider this earthquake as an independent event. The maximum and minimum ΔCFS changes caused by 2002 earthquake event are 0.9427MPa and -2.951MPa respectively.

5.3.11 The 2005 Earthquake (Main Shock)

We have calculated the time dependent sequence for the stress on active faults in the region after the 2002 earthquake since the post seismic stress after the earthquake will influence the accumulation of stress on these faults as a function of time. However, when the post-seismic viscoelastic relaxation process of 03 years between the 2002 and immediately preceding earthquake and the duration since the inception of earthquake sequence is taken into consideration, the CFS accumulation near the epicenter of 2002 earthquake rises time-dependently and reaches maximum CFS immediately before the occurrence of 2005 earthquake event in Figures 5.14, 5.15, 5.16, 5.17, 5.18, and 5.19(k).

The maximum and minimum CFS changes caused by the 2005 earthquake are respectively 23.83MPa and -7.28M Pa. The Figures show that co-seismic coulomb stress changes mostly on rupture fault of 2005 earthquake are less than 0.01MPa immediately after the 2002 earthquake but rise to more than 0.01MPa just before the 2005 earthquake due to post-seismic relaxation.

5.3.12 The 2005 Earthquake (Aftershock)

We have calculated the time dependent sequence for the stress on active faults in the region after the 2005(Main shock) earthquake, since the post seismic stress after the earthquake will influence the accumulation of stress on these faults as a function of time. However, when the post-seismic viscoelastic relaxation process of the same earthquake with gap of hours in time. It is immediately preceding earthquake and also the duration since the inception of earthquake sequence is taken into consideration, the CFS accumulation near the epicenter of 2005 earthquake rises time-dependently and reaches maximum CFS immediately before the occurrence of 2005(Aftershock) earthquake event in Figures 5.14, 5.15, 5.16, 5.17, 5.18, and 5.19(l). The maximum and minimum CFS changes caused by the 2005 earthquake are respectively

0.3734MPa and -1.337MPa. The co-seismic coulomb stress changes mostly on rupture fault of 2005(Aftershock) earthquake indicating that, this earthquake is triggered by the preceding event. One of the reasons of triggering of this earthquake is 2005 main shock zone which is one of the devastating earthquake in the Central Himalayas.

Based on our findings, we concluded that one of the twelve earthquakes could have been triggered by past events. The main Kashmir earthquake caused stress and rupture in the surrounding area, triggering the 2005 earthquake (After shock).

The stress maps show positive CFS (red lobes), indicating that these segments are vulnerable to seismic hazards.

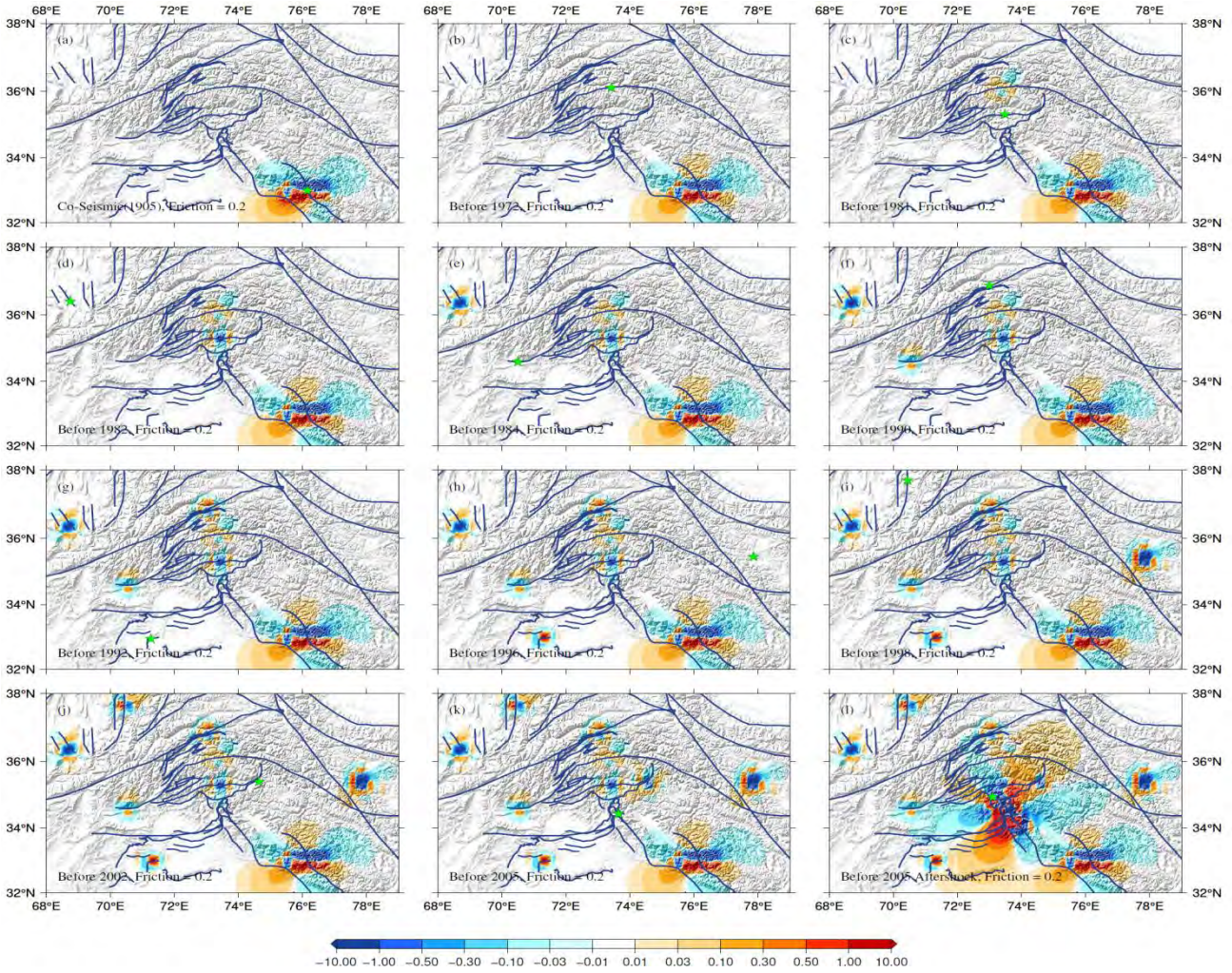

Figure 5.14 (a-l) The Post-seismic Coulomb stress changes caused by the 1905-2005 earthquake sequence. Active faults in the study are indicated by blue lines. The Green star indicates the portion of the current earthquake rupture in the area. Friction =0.2, Viscosity of lower Crust and upper Mantle= 1×10^{19} Pa s. Color bar is showing CFS changes.

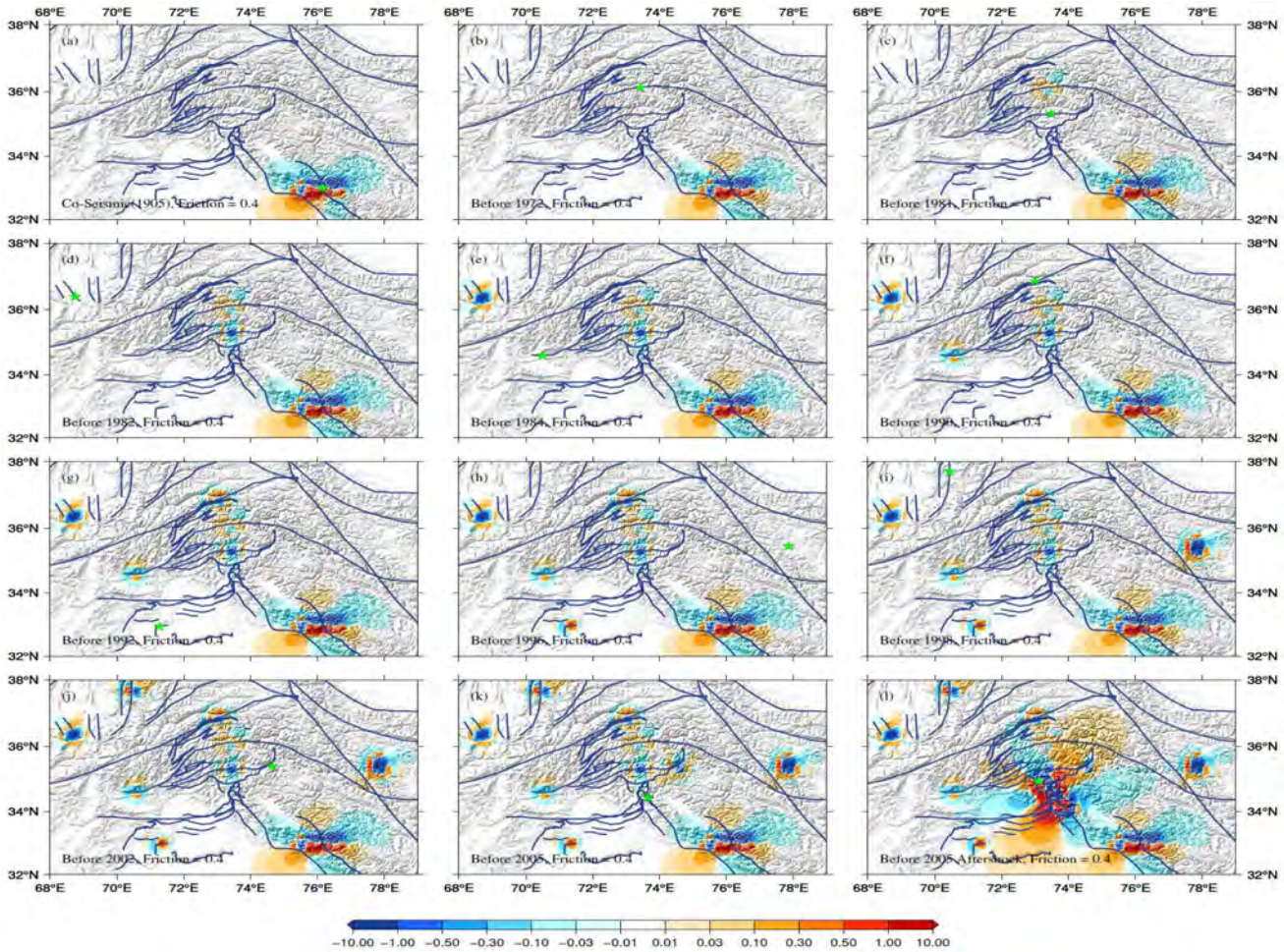

Figure 5.15 (a-l) The Post-seismic Coulomb stress changes caused by the 1905-2005 earthquake sequence. Active faults in the study are indicated by blue lines. The Green star indicates the portion of the current earthquake rupture in the area. Friction =0.4, Viscosity of lower Crust and upper Mantle= 1×10^{19} Pa s. Color bar is showing CFS changes.

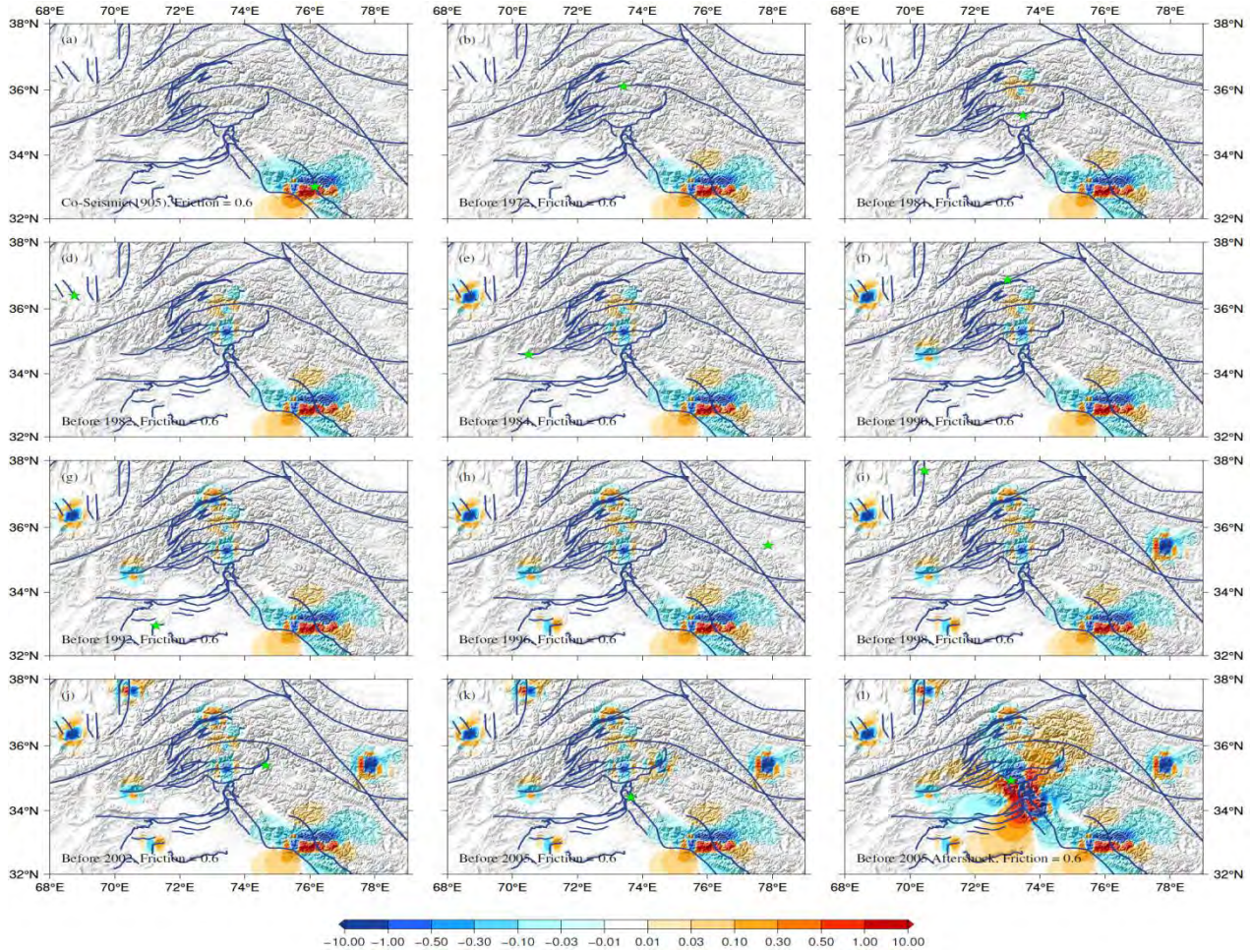

Figure 5.16 (a-l) The Post-seismic Coulomb stress changes caused by the 1905-2005 earthquake sequence. Active faults in the study are indicated by blue lines. The Green star indicates the portion of the current earthquake rupture in the area. Friction =0.6, Viscosity of lower Crust and upper Mantle= 1×10^{19} Pa s. Color bar is showing CFS changes.

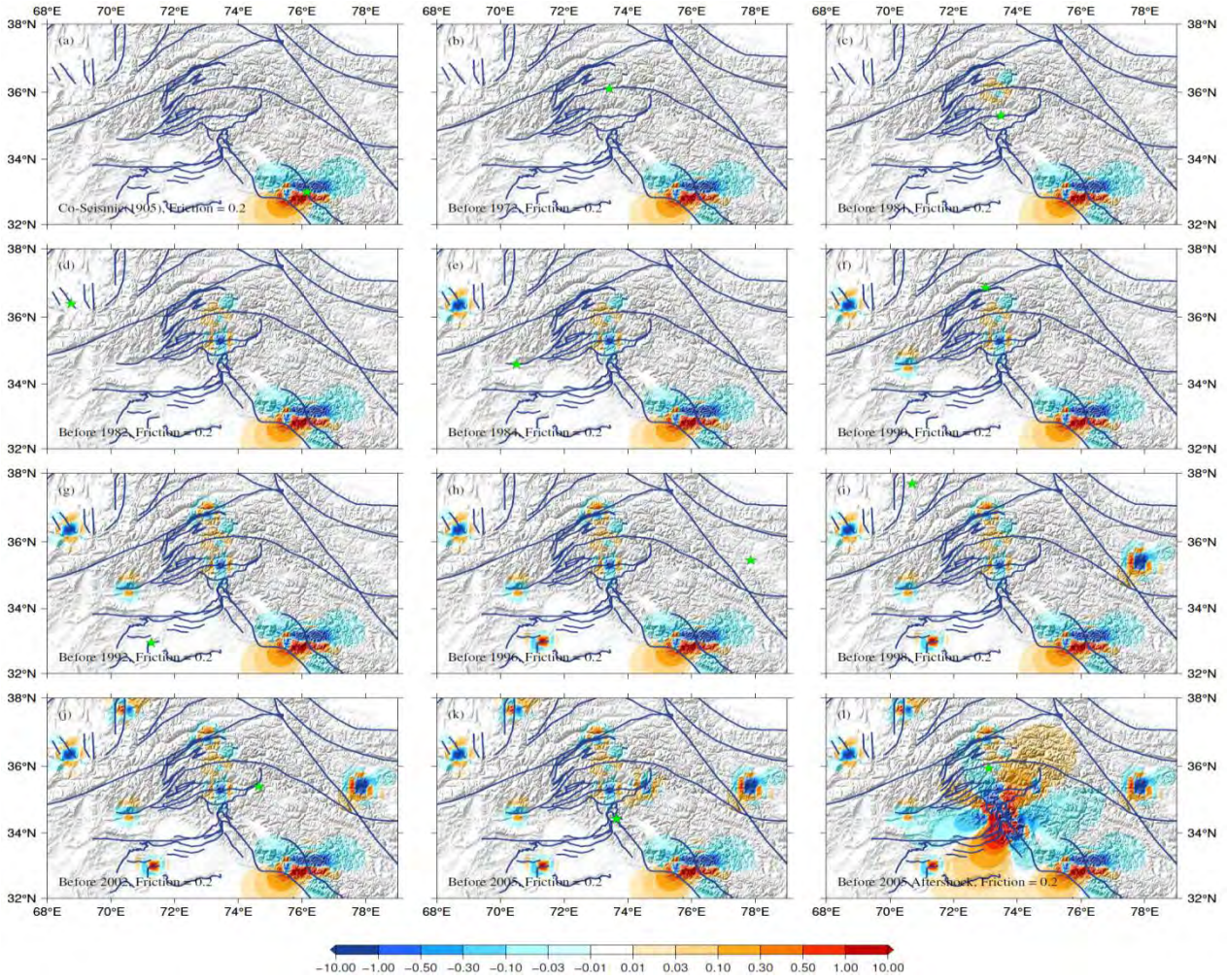

Figure 5.17 (a-l) The Post-seismic Coulomb stress changes caused by the 1905-2005 earthquake sequence. Active faults in the study are indicated by blue lines. The Green star indicates the portion of the current earthquake rupture in the area. Friction =0.2, Viscosity of lower Crust and upper Mantle= 1×10^{20} Pa s. Color bar is showing CFS changes

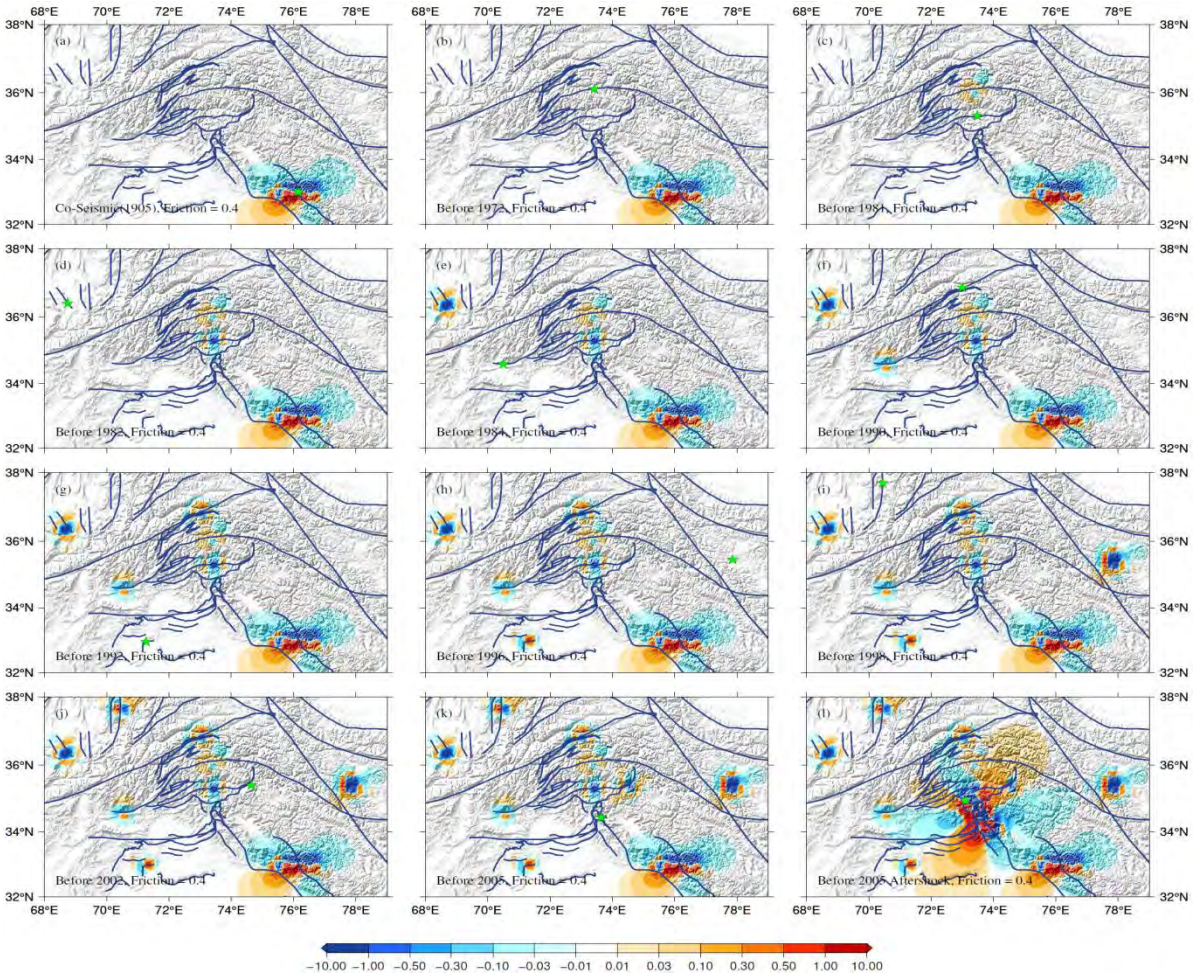

Figure 5.18 (a-l) The Post-seismic Coulomb stress changes caused by the 1905-2005 earthquake sequence. Active faults in the study are indicated by blue lines. The Green star indicates the portion of the current earthquake rupture in the area. Friction =0.4, Viscosity of lower Crust and upper Mantle= 1×10^{20} Pa s. Color bar is showing CFS changes.

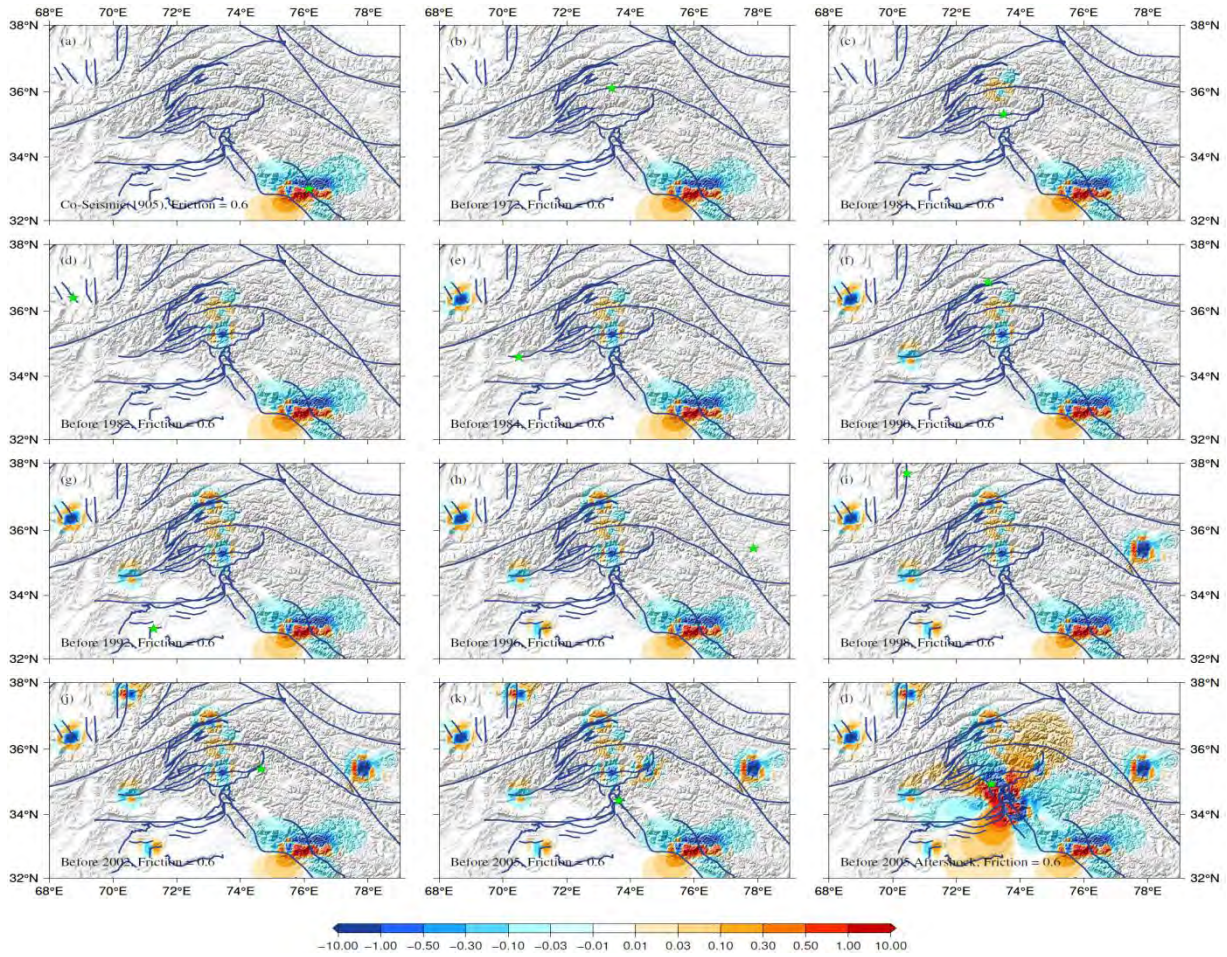

Figure 5.19 (a-l) The Post-seismic Coulomb stress changes caused by the 1905-2005 earthquake sequence. Active faults in the study are indicated by blue lines. The Green star indicates the portion of the current earthquake rupture in the area. Friction =0.6, Viscosity of lower Crust and upper Mantle= 1×10^{20} Pa s. Color bar is showing CFS changes.

Conclusion

The investigation of earthquake catalogues was carried out to analyze the different earthquake parameters such as FMS, Rupture Length, Rupture width, uniform slip as well as Co- and post-seismic stress transfer based on these parameters. Several simulations were adopted with varying values of the coefficient of friction and the viscosities of the lower crust and upper mantle to test the robustness of our numerical results which are given below:

1. Based on FMS solution, 6 out of 12 earthquakes are thrust in nature while others are strike-slip in nature with normal strike-slip component as well.

2. The statistical results give the exponential relation of earthquake's magnitude with their rupture length and width give the.

3. Based on simulations we conclude that co-seismic stress is not the only major driving force that resulted in the occurrence of subsequent events. However, the post-seismic visco-elastic relaxation process is more important in the stress transfer and accumulation that occurs after major earthquakes.

4. Our results showed a significant gap between earthquakes and faults in the study area. Only 2005 (Aftershock) out of selected 12 earthquakes, has been triggered by the preceding earthquake 2005(Main shock), which is further transferring the CFS in the Northern and Southern regions. The presence of CFS (red lobes) in the stress map with positive values indicates that these segments are susceptible to seismic hazards.

5. Based on our findings and a variety of simulations in the study area, we concluded that static earthquake stress transfer and visco-elastic stress transfer are inefficient in the area and do not play a significant role in earthquake occurrence.

6. As a result, tectonic loading plays an important role in the region's active seismicity.

References

Aki K, Richards PG (2002) Quantitative Seismology 2nd edn. University Science Books, California.

Ambraseys, N. & Bilham, R., 2003. Earthquakes and associated deformation in northern Baluchistan, Bull. seism. Soc. Am., 93, 1573–1605.

Ambraseys, N. N., & Douglas, J. (2004). Magnitude calibration of north Indian earthquakes. Geophysical Journal International, 159(1), 165-206.

Armbruster, J., Seeber, L., & Jacob, K. H. (1977). The northwestern termination of the Himalayan mountain front: Active tectonics from microearthquakes. J. Geophys. Res.

Armbruster, J., Seeber, L., & Jacob, K. H. (1978). The northwestern termination of the Himalayan mountain front: active tectonics from microearthquakes. Journal of Geophysical Research: Solid Earth, 83(B1), 269-282.

Barka, A. (1999). The 17 august 1999 Izmit earthquake. Science, 285(5435), 1858-1859.

Freed, A. M. (2005). EARTHQUAKE TRIGGERING BY STATIC, DYNAMIC, AND POSTSEISMIC STRESS TRANSFER. Annual Review of Earth and Planetary Sciences, 33(1), 335-367. doi: 10.1146/annurev.earth.33.092203.12250.

Glasser, R. (2020). The climate change imperative to transform disaster risk management. International Journal of Disaster Risk Science, 11(2), 152-154.

Gomberg, J., & Felzer, K. (2008). A model of earthquake triggering probabilities and application to dynamic deformations constrained by ground motion observations. Journal of Geophysical Research: Solid Earth, 113(B10).

Harris, R. A. (1998). Introduction to special section: Stress triggers, stress shadows, and implications for seismic hazard. Journal of Geophysical Research: Solid Earth, 103(B10), 24347-24358.

Hodges, K. V. (2000). Tectonics of the Himalaya and southern Tibet from two perspectives. Geological Society of America Bulletin, 112(3), 324-350.

Kagan, Y. Y. (1991). Likelihood analysis of earthquake catalogueues. Geophysical journal international, 106(1), 135-148.

Kazmi, A., & Qasim Jan, M. (1997). Geology and tectonics of Pakistan. Graphic Publishers.

King GCP, Stein RS, Lin J (1994) Static stress changes and the triggering of earthquakes. Bull Seismol Soc Am 84:935–953.

Malik, J. N., Sahoo, S., Satuluri, S., & Okumura, K. (2015). Active fault and paleoseismic studies in Kangra valley: Evidence of surface rupture of a great Himalayan 1905 Kangra earthquake (M w 7.8), Northwest Himalaya, India. Bulletin of the Seismological Society of America, 105(5), 2325-2342.

MonaLisa, Khwaja, A., & Jan, M. (2007). Seismic Hazard Assessment of the NW Himalayan Fold-and-Thrust Belt, Pakistan, Using Probabilistic Approach. Journal Of Earthquake Engineering, 11(2), 257-301.

Navas-Portella, V., Jiménez, A., & Corral, Á. (2020). No significant effect of Coulomb stress on the Gutenberg-Richter Law after the Landers Earthquake. Scientific reports, 10(1), 1-13.

Pecher, A., Seeber, L., Guillot, S., Jouanne, F., Kausar, A., Latif, M., ... & Van Melle, J. (2008). Stress field evolution in the northwest Himalayan syntaxis, northern Pakistan. Tectonics, 27(6).

Rehman, K., & Burton, P. W. (2020). Seismicity and seismic hazard parameters in and around Pakistan. Journal of Seismology, 24(3), 635-653.

Ryder, I., Parsons, B., Wright, T. J., & Funning, G. J. (2007). Post-seismic motion following the 1997 Manyi (Tibet) earthquake: InSAR observations and modelling. Geophysical Journal International, 169(3), 1009-1027.

Sahoo, S., & Malik, J. (2017). Active fault topography along Kangra Valley Fault in the epicentral zone of 1905 Mw7.8 earthquake NW Himalaya, India. Quaternary International, 462, 90-108.

Scholz CH (1990) The Mechanics of earthquakes and faulting. Cambridge Univ Press, New York, p 439.

Seeber, L. and Armbruster. J., 1979. Seismicity of Hazara Arc in Northern

Shao, Z., Xu, J., Ma, H., & Zhang, L. (2016). Coulomb stress evolution over the past 200 years and seismic hazard along the Xianshuihe fault zone of Sichuan, China. Tectonophysics, 670, 48-65.

Sorkhabi, R. (2010). The HJ/66/9 Geologic Formation of the Himalaya. The HJ/66/9 Geologic Formation of the Himalaya.

Steacy, S., Gomberg, J., & Cocco, M. (2005). Introduction to special section: Stress transfer, earthquake triggering, and time‐dependent seismic hazard. Journal of Geophysical Research: Solid Earth, 110(B5).

Stein, R., King, G., & Lin, J. (1992). Change in Failure Stress on the Southern San Andreas Fault System Caused by the 1992 Magnitude = 7.4 Landers Earthquake. Science, 258(5086), 1328-1332.

Stein, R. S. (1999). The role of stress transfer in earthquake occurrence. Nature, 402(6762), 605-609.

Sultan M (2015) Seismic Hazard Analysis of Pakistan. J Geol Geosci 4: 190.

Treloar, P. J., Searle, M. P., Khan, M. A., & Jan, M. Q. (2000). Tectonics of the Nanga Parbat syntaxis and the western Himalaya: an introduction. Geological Society, London, Special Publications, 170(1), 1-6.

Verdecchia, A., & Carena, S. (2015). One hundred and fifty years of Coulomb stress history along the California‐Nevada border, USA. Tectonics, 34(2), 213-231.

Wadia, D. N. (1931). The syntaxis of the northwest Himalaya: its rocks, tectonics and orogeny. Rec. Geol. Surv. India, 65(2), 189-220.

Wang, R., Lorenzo-Martín, F., & Roth, F. (2006). PSGRN/PSCMP—a new code for calculating co-and post-seismic deformation, geoid and gravity changes based on the viscoelastic-gravitational dislocation theory. Computers & Geosciences, 32(4), 527-541.

Wang, Z. (2011). Seismic hazard assessment: issues and alternatives. Pure and Applied Geophysics, 168(1-2), 11-25.

Wells, D. L., & Coppersmith, K. J. (1994). New empirical relationships among magnitude, rupture length, rupture width, rupture area, and surface displacement. Bulletin of the seismological Society of America, 84(4), 974-1002.

Xiong, X., Shan, B., Zhou, Y. M., Wei, S. J., Li, Y. D., Wang, R. J., & Zheng, Y. (2017). Coulomb stress transfer and accumulation on the Sagaing Fault, Myanmar, over the past 110 years and its implications for seismic hazard. Geophysical Research Letters, 44(10), 4781-4789.

Appendices

This portion contains all input files of computer program which have been used in making Rupture Models and Simulations.

```
#=============================================================================
# This is input file of FORTRAN77 program "pscmp08" for modeling post-seismic
# deformation induced by earthquakes in multi-layered viscoelastic media using
# the Green's function approach. The earthquke source is represented by an
# arbitrary number of rectangular dislocation planes. For more details, please
# read the accompanying READ.ME file.
#
# written by Rongjiang Wang
# GeoForschungsZentrum Potsdam
# e-mail: wang@gfz-potsdam.de
# phone +49 331 2881209
# fax +49 331 2881204
#
# Last modified: Potsdam, July, 2008
#
# References:
#
# (1) Wang, R., F. Lorenzo-Martín and F. Roth (2003), Computation of deformation
#     induced by earthquakes in a multi-layered elastic crust - FORTRAN programs
#     EDGRN/EDCMP, Computer and Geosciences, 29(2), 195-207.
# (2) Wang, R., F. Lorenzo-Martin and F. Roth (2006), PSGRN/PSCMP - a new code for
#     calculating co- and post-seismic deformation, geoid and gravity changes
#     based on the viscoelastic-gravitational dislocation theory, Computers and
#     Geosciences, 32, 527-541. DOI:10.1016/j.cageo.2005.08.006.
# (3) Wang, R. (2005), The dislocation theory: a consistent way for including the
#     gravity effect in (visco)elastic plane-earth models, Geophysical Journal
#     International, 161, 191-196.
```

```
#
#########################################################################
##                                                                     ##
## Green's functions should have been prepared with the                ##
## program "psgrn08" before the program "pscmp08" is started.          ##
##                                                                     ##
## For local Cartesian coordinate system, the Aki's convention         ##
## is used, that is, x is northward, y is eastward, and z is           ##
## downward.                                                           ##
##                                                                     ##
## If not specified otherwise, SI Unit System is used overall!         ##
##                                                                     ##
#########################################################################
#=======================================================================
===========
# OBSERVATION ARRAY
# =================
# 1. selection for irregular observation positions (= 0) or a 1D
observation
#    profile (= 1) or a rectangular 2D observation array (= 2):
iposrec
#
#    IF (iposrec = 0 for irregular observation positions) THEN
#
# 2. number of positions: nrec
#
# 3. coordinates of the observations: (lat(i),lon(i)), i=1,nrec
#
#    ELSE IF (iposrec = 1 for regular 1D observation array) THEN
#
# 2. number of position samples of the profile: nrec
#
# 3. the start and end positions: (lat1,lon1), (lat2,lon2)
#
#    ELSE IF (iposrec = 2 for rectanglular 2D observation array) THEN
#
# 2. number of x samples, start and end values: nxrec, xrec1, xrec2
#
# 3. number of y samples, start and end values: nyrec, yrec1, yrec2
#
#    sequence of the positions in output data: lat(1),lon(1); ...;
lat(nx),lon(1);
#    lat(1),lon(2); ...; lat(nx),lon(2); ...; lat(1),lon(ny); ...;
lat(nx),lon(ny).
```

```
#
#    Note that the total number of observation positions (nrec or
nxrec*nyrec)
#    should be <= NRECMAX (see pecglob.h)!
#=====================================================================
==========
#  0
#  6
#   ( 5.0,50.0), (25.0,50.0), (10.0, 50.0)
#   ( 0.0,  1.5), ( 0.0, 3.0), ( 0.0, 10.0)
#
#  1
#  51
#  (0.0,  10.0), (0.0, 15.0)
#
  2
 61     30.0        40.0
 61     66.0        80.0
#=====================================================================
==========
# OUTPUTS
# =======
#
# 1. select output for los displacement (only for snapshots, see
below), x, y,
#    and z-cosines to the INSAR orbit: insar (1/0 = yes/no), xlos,
ylos, zlos
#
#    if this option is selected (insar = 1), the snapshots will
include additional
#    data:
#    LOS_Dsp = los displacement to the given satellite orbit.
#
# 2. select output for Coulomb stress changes (only for snapshots,
see below):
#    icmb (1/0 = yes/no), friction, Skempton ratio, strike, dip, and
rake angles
#    [deg] describing the uniform regional master fault mechanism,
the uniform
#    regional principal stresses: sigma1, sigma2 and sigma3 [Pa] in
arbitrary
#    order (the orietation of the pre-stress field will be derived by
assuming
```

```
#    that the master fault is optimally oriented according to Coulomb
failure
#    criterion)
#
#    if this option is selected (icmb = 1), the snapshots will
include additional
#    data:
#    CMB_Fix, Sig_Fix = Coulomb and normal stress changes on master
fault;
#    CMB_Op1/2, Sig_Op1/2 = Coulomb and normal stress changes on the
two optimally
#                         oriented faults;
#    Str_Op1/2, Dip_Op1/2, Slp_Op1/2 = strike, dip and rake angles of
the two
#                         optimally oriented faults.
#
#    Note: the 1. optimally orieted fault is the one closest to the
master fault.
#
# 3. output directory in char format: outdir
#
# 4. select outputs for displacement components (1/0 = yes/no):
itout(i), i=1-3
#
# 5. the file names in char format for the x, y, and z components:
#    toutfile(i), i=1-3
#
# 6. select outputs for stress components (1/0 = yes/no): itout(i),
i=4-9
#
# 7. the file names in char format for the xx, yy, zz, xy, yz, and zx
components:
#    toutfile(i), i=4-9
#
# 8. select outputs for vertical NS and EW tilt components, block
rotation, geoid
#    and gravity changes (1/0 = yes/no): itout(i), i=10-14
#
# 9. the file names in char format for the NS tilt (positive if
borehole top
#    tilts to north), EW tilt (positive if borehole top tilts to
east), block
#    rotation (clockwise positive), geoid and gravity changes:
toutfile(i), i=10-14
```

```
#
#    Note that all above outputs are time series with the time window
as same
#    as used for the Green's functions
#
#10. number of scenario outputs ("snapshots": spatial distribution of
all above
#    observables at given time points; <= NSCENMAX (see pscglob.h):
nsc
#
#11. the time [day], and file name (in char format) for the 1.
snapshot;
#12. the time [day], and file name (in char format) for the 2.
snapshot;
#13. ...
#
#    Note that all file or directory names should not be longer than
80
#    characters. Directories must be ended by / (unix) or \ (dos)!
#=============================================================
===========
 0    -0.072  0.408  -0.910
 1     0.400  0.000  331.00   29.00   125.0    1.0E+06   -1.0E+06
0.0E+00
'./out-cmb/'
  0           0           0
  'ux.dat'    'uy.dat'    'uz.dat'
  0           0           0           0           0           0
  'sxx.dat'   'syy.dat'   'szz.dat'   'sxy.dat'    'syz.dat'
'szx.dat'
  0           0           0           0           0
  'tx.dat'    'ty.dat'    'rot.dat'   'gd.dat'    'gr.dat'
  1
     0.00  '2005M-coseismF04_RUP_SD_RAD.dat'           |0 co-seismic
#   730.00  'snapshot_2_year.dat'       |2 years
#  1825.00  'snapshot_5_year.dat'       |5 years
#=============================================================
===========
#
# GREEN'S FUNCTION DATABASE
# =========================
# 1. directory where the Green's functions are stored: grndir
#
# 2. file names (without extensions!) for the 13 Green's functions:
```

```
#    3 displacement komponents (uz, ur, ut): green(i), i=1-3
#    6 stress components (szz, srr, stt, szr, srt, stz): green(i),
i=4-9
#    radial and tangential components measured by a borehole
tiltmeter,
#    rigid rotation around z-axis, geoid and gravity changes (tr, tt,
rot, gd, gr):
#    green(i), i=10-14
#
#    Note that all file or directory names should not be longer than
80
#    characters. Directories must be ended by / (unix) or \ (dos)!
The
#    extensions of the file names will be automatically considered.
They
#    are ".ep", ".ss", ".ds" and ".cl" denoting the explosion
(inflation)
#    strike-slip, the dip-slip and the compensated linear vector
dipole
#    sources, respectively.
#
#=======================================================================
==========
  './grn_NP_10km/'
 'uz'  'ur'  'ut'
 'szz' 'srr' 'stt' 'szr' 'srt' 'stz'
 'tr'  'tt'  'rot' 'gd'  'gr'
#=======================================================================
==========
# RECTANGULAR SUBFAULTS
# ====================
# 1. number of subfaults (<= NSMAX in pscglob.h): ns
#
# 2. parameters for the 1. rectangular subfault: geographic
coordinates
#    (0_lat, 0_lon) [deg] and 0_depth [km] of the local reference
point on
#    the present fault plane, length (along strike) [km] and width
(along down
#    dip) [km], strike [deg], dip [deg], number of equi-size fault
patches along
#    the strike (np_st) and along the dip (np_di) (total number of
fault patches
```

```
#    = np_st x np_di), and the start time of the rupture; the
following data
#    lines describe the slip distribution on the present sub-fault:
#
#    pos_s[km]  pos_d[km]  slip_strike[m]  slip_downdip[m]  opening[m]
#
#    where (pos_s,pos_d) defines the position of the center of each
patch in
#    the local coordinate system with the origin at the reference
point:
#    pos_s = distance along the length (positive in the strike
direction)
#    pos_d = distance along the width (positive in the down-dip
direction)
#
#
# 3. ... for the 2. subfault ...
# ...
#                  N
#                 /
#                /| strike
#               +-----------------------
#               |\        p .          \ W
#               :-\      i .            \ i
#               |  \     l .             \ d
#               :90 \  S .                \ t
#               |-dip\  .                  \ h
#               :     \.| rake              \
#               Z       ------------------------
#                             L e n g t h
#
#    Simulation of a Mogi source:
#    (1) Calculate deformation caused by three small openning plates
(each
#        causes a third part of the volume of the point inflation)
located
#        at the same depth as the Mogi source but oriented orthogonal
to
#        each other.
#    (2) Multiply the results by 3(1-nu)/(1+nu), where nu is the
Poisson
#        ratio at the source depth.
#    The multiplication factor is the ratio of the seismic moment
(energy) of
```

```
#    the Mogi source to that of the plate openning with the same
volume change.
#=================================================================
==========
# n_faults
#-----------------------------------------------------------------
----------
  84
#-----------------------------------------------------------------
----------
# n   O_lat   O_lon   O_depth length  width strike dip   np_st np_di
start_time
# [-] [deg]   [deg]   [km]    [km]     [km] [deg]  [deg] [-]   [-]
[day]
#     pos_s   pos_d   slp_stk slp_ddip open
#     [km]    [km]    [m]     [m]      [m]
#-----------------------------------------------------------------
----------
1     33.9704     73.7238     0.393 9     9     331   29    1     1
      0
      0     0     0.296349165 0.95371844  0
2     34.0412     73.6762     0.393 9     9     331   29    1     1
      0
      0     0     0.576602342 1.855682079 0
3     34.1121     73.6285     0.393 9     9     331   29    1     1
      0
      0     0     0.100865862 2.741745254 0
4     34.1829     73.5809     0.393 9     9     331   29    1     1
      0
      0     0     -0.490407287      3.726872911 0
5     34.2538     73.5333     0.393 9     9     331   29    1     1
      0
      0     0     -1.010867462      4.363950873 0
6     34.3246     73.4856     0.393 9     9     331   29    1     1
      0
      0     0     -2.492546119      4.56596297  0
7     34.3954     73.438      0.393 9     9     331   29    1     1
      0
      0     0     -3.086467024      4.705101032 0
8     34.4663     73.3904     0.393 9     9     331   29    1     1
      0
      0     0     -2.582375993      5.085058945 0
9     34.5371     73.3427     0.393 9     9     331   29    1     1
      0
```

	0	0	-1.538795686		5.067412027	0				
10	34.608		73.2951	0.393	9	9	331	29	1	1
	0									
	0	0	-0.824400203		4.005338787	0				
11	34.6788		73.2475	0.393	9	9	331	29	1	1
	0									
	0	0	-0.161326365		2.690367418	0				
12	34.7496		73.1998	0.393	9	9	331	29	1	1
	0									
	0	0	0.300846523	1.645117968	0					
13	34.8205		73.1522	0.393	9	9	331	29	1	1
	0									
	0	0	0.235329906	0.80698711	0					
14	34.8913		73.1045	0.393	9	9	331	29	1	1
	0									
	0	0	0.095080038	0.306071947	0					
15	34.0048		73.799	3.9702		9	9	331	29	1
	1	0								
	0	0	0.295549558	0.953128989	0					
16	34.0756		73.7513	3.9702		9	9	331	29	1
	1	0								
	0	0	0.536989358	1.787690686	0					
17	34.1464		73.7037	3.9702		9	9	331	29	1
	1	0								
	0	0	-0.252486582		3.062609921	0				
18	34.2173		73.6561	3.9702		9	9	331	29	1
	1	0								
	0	0	-0.304370718		4.383044538	0				
19	34.2881		73.6084	3.9702		9	9	331	29	1
	1	0								
	0	0	-0.856461391		4.954721902	0				
20	34.3589		73.5608	3.9702		9	9	331	29	1
	1	0								
	0	0	-2.668264481		4.954593366	0				
21	34.4298		73.5132	3.9702		9	9	331	29	1
	1	0								
	0	0	-3.262175614		5.330756077	0				
22	34.5006		73.4655	3.9702		9	9	331	29	1
	1	0								
	0	0	-2.992129467		5.622168149	0				
23	34.5715		73.4179	3.9702		9	9	331	29	1
	1	0								
	0	0	-1.592484443		5.827736032	0				

24	34.6423	73.3703	3.9702	9	9	331	29	1
	1	0						
	0	0	-0.871619975	4.434858138	0			
25	34.7131	73.3226	3.9702	9	9	331	29	1
	1	0						
	0	0	-0.252796139	2.868883775	0			
26	34.784	73.275	3.9702	9	9	331	29	1
	1	0						
	0	0	0.353161404	1.717363652	0			
27	34.8548	73.2273	3.9702	9	9	331	29	1
	1	0						
	0	0	0.204927505	0.659913417	0			
28	34.9257	73.1797	3.9702	9	9	331	29	1
	1	0						
	0	0	0.070012582	0.225794593	0			
29	34.0391	73.8741	8.3335	9	9	331	29	1
	1	0						
	0	0	0.124912467	0.41291989	0			
30	34.1099	73.8265	8.3335	9	9	331	29	1
	1	0						
	0	0	0.181651679	0.700221556	0			
31	34.1808	73.7789	8.3335	9	9	331	29	1
	1	0						
	0	0	-0.268736045	1.549671184	0			
32	34.2516	73.7312	8.3335	9	9	331	29	1
	1	0						
	0	0	-0.125756198	2.56411802	0			
33	34.3225	73.6836	8.3335	9	9	331	29	1
	1	0						
	0	0	-0.94181116	2.563038841	0			
34	34.3933	73.636	8.3335	9	9	331	29	1
	1	0						
	0	0	-1.771266303	2.444168148	0			
35	34.4641	73.5883	8.3335	9	9	331	29	1
	1	0						
	0	0	-2.491457257	3.003299115	0			
36	34.535	73.5407	8.3335	9	9	331	29	1
	1	0						
	0	0	-1.894252844	3.491671222	0			
37	34.6058	73.493	8.3335	9	9	331	29	1
	1	0						
	0	0	-1.043205324	3.71739743	0			
38	34.6766	73.4454	8.3335	9	9	331	29	1
	1	0						

	0	0	-0.758830583	2.484395588	0					
39	34.7475	73.3978	8.3335	9	9	331	29	1		
	1	0								
	0	0	-0.359529827	1.481704557	0					
40	34.8183	73.3501	8.3335	9	9	331	29	1		
	1	0								
	0	0	0.023467042	0.891591222	0					
41	34.8892	73.3025	8.3335	9	9	331	29	1		
	1	0								
	0	0	-0.072575351	0.138202852	0					
42	34.96	73.2549	8.3335	9	9	331	29	1	1	
	0									
	0	0	-0.052242827	0.016872967	0					
43	34.0734	73.9493	12.6968	9	9	331	29	1		
	1	0								
	0	0	-0.15972672	0.050101247	0					
44	34.1443	73.9017	12.6968	9	9	331	29	1		
	1	0								
	0	0	-0.250384289	0.078160077	0					
45	34.2151	73.854	12.6968	9	9	331	29	1		
	1	0								
	0	0	-0.485311012	0.231272527	0					
46	34.286	73.8064	12.6968	9	9	331	29	1		
	1	0								
	0	0	-0.602908789	0.677070566	0					
47	34.3568	73.7588	12.6968	9	9	331	29	1		
	1	0								
	0	0	-1.015268426	0.444475999	0					
48	34.4276	73.7111	12.6968	9	9	331	29	1		
	1	0								
	0	0	-0.907555055	0.437492939	0					
49	34.4985	73.6635	12.6968	9	9	331	29	1		
	1	0								
	0	0	-0.672765966	0.716711208	0					
50	34.5693	73.6158	12.6968	9	9	331	29	1		
	1	0								
	0	0	-0.389237493	1.428934979	0					
51	34.6401	73.5682	12.6968	9	9	331	29	1		
	1	0								
	0	0	-0.34183284	1.632801748	0					
52	34.711	73.5206	12.6968	9	9	331	29	1		
	1	0								
	0	0	-0.764511258	0.643057958	0					

53 34.7818 73.4729 12.6968 9 9 331 29 1
1 0
0 0 -0.579439344 0.246008733 0
54 34.8527 73.4253 12.6968 9 9 331 29 1
1 0
0 0 -0.392996226 0.272450373 0
55 34.9235 73.3777 12.6968 9 9 331 29 1
1 0
0 0 -0.41537893 0.129171765 0
56 34.9943 73.33 12.6968 9 9 331 29 1 1
0
0 0 -0.167872709 0.052531548 0
57 34.1078 74.0245 17.0601 9 9 331 29 1
1 0
0 0 -0.174271329 0.054518474 0
58 34.1786 73.9768 17.0601 9 9 331 29 1
1 0
0 0 -0.503237106 0.15646538 0
59 34.2495 73.9292 17.0601 9 9 331 29 1
1 0
0 0 -0.550595519 0.17120787 0
60 34.3203 73.8815 17.0601 9 9 331 29 1
1 0
0 0 -0.759314882 0.236186262 0
61 34.3911 73.8339 17.0601 9 9 331 29 1
1 0
0 0 -0.815086093 0.253510594 0
62 34.462 73.7863 17.0601 9 9 331 29 1
1 0
0 0 -0.482115059 0.151638486 0
63 34.5328 73.7386 17.0601 9 9 331 29 1
1 0
0 0 0.068117847 0.222402156 0
64 34.6037 73.691 17.0601 9 9 331 29 1
1 0
0 0 0.11290399 0.363677507 0
65 34.6745 73.6434 17.0601 9 9 331 29 1
1 0
0 0 -0.080576155 0.438559338 0
66 34.7453 73.5957 17.0601 9 9 331 29 1
1 0
0 0 -0.482978877 0.150216658 0
67 34.8162 73.5481 17.0601 9 9 331 29 1
1 0

	0	0	-0.473896604	0.147766601	0				
68	34.887	73.5005	17.0601	9	9	331	29	1	
	1	0							
	0	0	-0.553746389	0.172188694	0				
69	34.9578	73.4528	17.0601	9	9	331	29	1	
	1	0							
	0	0	-0.59278699	0.184380653	0				
70	35.0287	73.4052	17.0601	9	9	331	29	1	
	1	0							
	0	0	-0.198181818	0.061820119	0				
71	34.1421	74.0996	21.4234	9	9	331	29	1	
	1	0							
	0	0	-0.113725417	0.035374278	0				
72	34.213	74.052	21.4234	9	9	331	29	1	
	1	0							
	0	0	-0.47618888	0.148141286	0				
73	34.2838	74.0043	21.4234	9	9	331	29	1	
	1	0							
	0	0	-0.477301962	0.148939039	0				
74	34.3546	73.9567	21.4234	9	9	331	29	1	
	1	0							
	0	0	-0.476882391	0.148268491	0				
75	34.4255	73.9091	21.4234	9	9	331	29	1	
	1	0							
	0	0	-0.477150735	0.148415855	0				
76	34.4963	73.8614	21.4234	9	9	331	29	1	
	1	0							
	0	0	-0.477439012	0.148499125	0				
77	34.5672	73.8138	21.4234	9	9	331	29	1	
	1	0							
	0	0	-0.433017994	0.136756085	0				
78	34.638	73.7662	21.4234	9	9	331	29	1	
	1	0							
	0	0	-0.463740931	0.14439127	0				
79	34.7088	73.7185	21.4234	9	9	331	29	1	
	1	0							
	0	0	-0.476832679	0.148428288	0				
80	34.7797	73.6709	21.4234	9	9	331	29	1	
	1	0							
	0	0	-0.476113036	0.148048427	0				
81	34.8505	73.6233	21.4234	9	9	331	29	1	
	1	0							
	0	0	-0.446944419	0.139134095	0				

```
82      34.9214         73.5756         21.4234         9       9       331     29      1
        1       0
        0       0       -0.477134413            0.14846832      0
83      34.9922         73.528          21.4234         9       9       331     29      1
        1       0
        0       0       -0.477051881            0.148396978     0
84      35.063          73.4804         21.4234         9       9       331     29      1
        1       0
        0       0       -0.191249085            0.059530475     0
#============================end of Input======================
```